Complex seasonal cycle of ecohydrology in the Southwest United States

Michael Notaro,[1] Zhengyu Liu,[1] Robert G. Gallimore,[1] John W. Williams,[1,2] David S. Gutzler,[3] and Scott Collins[4]

Received 5 April 2010; revised 30 August 2010; accepted 27 September 2010; published 15 December 2010.

[1] This study investigates the causes for, and distribution of, unimodal versus bimodal seasonal cycle of vegetation greenness in the Southwest United States using extensive site observations, climate data, satellite data, and the Lund-Potsdam-Jena (LPJ) vegetation model. Peak vegetation greenness is achieved in a clockwise manner across the Southwest, beginning in spring in the Sonoran Desert following winter rains, then in Utah-Colorado with snowmelt/summer rains, and finally in New Mexico–eastern Arizona with late summer monsoon rains. At high elevations, spring-summer snowmelt is critical for supplying the necessary soil moisture to trigger vegetation growth. A bimodal seasonal cycle of vegetation greenness is evident in satellite data and LPJ simulations across eastern Arizona and western New Mexico, characterized by peaks during late spring–early summer and late summer–early autumn. This bimodal green-up remains a pressing paradox for which many competing hypotheses exist. The mechanism for this seasonal pattern is demonstrated using LPJ and observational data and is found to deviate from the traditional pulse-reserve paradigm. This paradigm states that rainfall events in arid lands produce nearly immediate pulses of vegetation growth and accumulation of reserves but does not consider cold dormancy, time-lagged vegetation responses, or rainfall seasonality. The following soil moisture based mechanism for bimodal greening is proposed. The initial peak in vegetation greenness during late spring–early summer results from a break in cold dormancy and benefits from the gradual winter-long accumulation of deep soil moisture from weak synoptic rain events and snowmelt in colder regions. Limited precipitation and ongoing transpiration, from the initial vegetation greening, trigger a midsummer drying of the soil and a consequential minimum in vegetation activity. Later, pulses of monsoon rainfall in late summer–early autumn support the secondary greening, although significant runoff of brief, intense rainstorms and substantial soil evaporation limit moisture to the upper soil layers.

Citation: Notaro, M., Z. Liu, R. G. Gallimore, J. W. Williams, D. S. Gutzler, and S. Collins (2010), Complex seasonal cycle of ecohydrology in the Southwest United States, *J. Geophys. Res.*, *115*, G04034, doi:10.1029/2010JG001382.

1. Introduction

[2] The Southwest United States (SWUS), defined here as Arizona, New Mexico, Utah, and Colorado, experiences complex, poorly understood [*Vivoni et al.*, 2008, 2010] seasonally varying interactions among vegetation, soil moisture, snow cover, and the atmosphere. The terrain (Figure 1), climate, and ecosystems vary dramatically across this region. The SWUS deserts contain more plant diversity than any other North American ecosystem [*Shreve*, 1942; *Whittaker and Niering*, 1965]. The water budget of the northern part of the region, particularly at higher elevations, is largely dominated by spring-summer snowmelt [*Hawkins and Ellis*, 2007]. Much of Utah and Arizona is characterized by dual precipitation peaks [*Guirguis and Avissar*, 2008], with a lesser winter-spring peak associated with large-scale weather systems and a greater summertime peak from convective storms. The North American monsoon dominates the precipitation seasonal cycle in New Mexico and eastern Arizona, with a unimodal summertime rainfall peak.

[3] Across the semiarid SWUS ecosystems, precipitation is the principal factor controlling primary productivity and ecosystem structure/dynamics [*Lange et al.*, 1976; *Hadley and Szarek*, 1981], and soil moisture is the dominant control on water and carbon exchange between land and atmosphere [*Vivoni et al.*, 2008; *Kurc and Small*, 2007]. The

[1]Center for Climatic Research, University of Wisconsin-Madison, Madison, Wisconsin, USA.
[2]Department of Geography, University of Wisconsin-Madison, Madison, Wisconsin, USA.
[3]Department of Earth and Planetary Sciences, University of New Mexico, Albuquerque, New Mexico, USA.
[4]Department of Biology, University of New Mexico, Albuquerque, New Mexico, USA.

0148-0227/10/2010JG001382

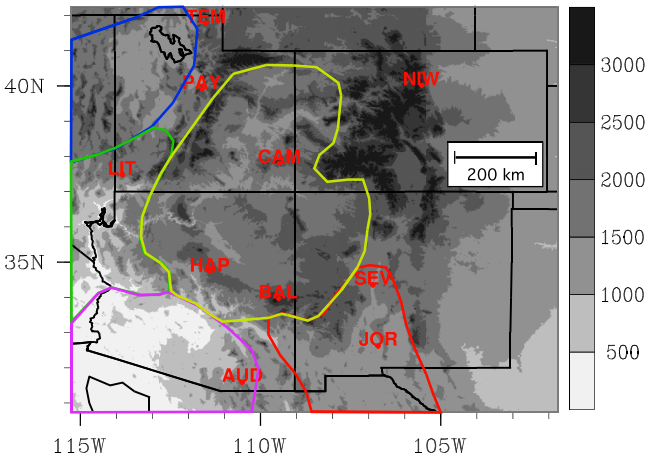

Figure 1. Elevation map (meters) of the entire study region with the location of 10 study sites. Elevation data with 30 s resolution is from the Shuttle Radar Topography Mission, obtained through Scripps Institution of Oceanography (topex.ucsd.edu/WWW_html/srtm30_plus.html). Elevation at the 10 sites ranges from approximately 1188 m at Jornada Basin (JOR) to 3050 m at Niwot Ridge (NIW). The approximate extent of the Great Basin Desert (blue), Mojave Desert (green), Sonoran Desert (purple), Chihuahuan Desert (red), and Colorado Plateau (yellow) is shown with colored curves.

interannual variability in winter-spring precipitation is partly linked to El Niño–Southern Oscillation (ENSO) and the Pacific Decadal Oscillation (PDO), with drought conditions associated with cold equatorial Pacific sea surface temperatures (SSTs) [*Andrade and Sellers*, 1988; *Gutzler et al.*, 2002; *Seager et al.*, 2005]. Known controls on the North American monsoon summer precipitation [*Vera et al.*, 2006] include SSTs off the northern Baja coast and in the Gulf of Mexico [*Carleton et al.*, 1990; *Huang and Lai*, 1998], southern Rockies snowpack [*Gutzler and Preston*, 1997; *Gutzler*, 2000], soil moisture [*Higgins et al.*, 1998; *Small*, 2001], ENSO [*Yu and Wallace*, 2000; *Higgins and Shi*, 2001], moisture transport from the Gulf of California and Great Plains low-level jets [*Bosilovich and Schubert*, 2002], and large-scale teleconnection patterns [*Carleton et al.*, 1990].

[4] Through its influence on evapotranspiration, respiration, and carbon assimilation, soil moisture serves as a critical link between hydrological and ecological processes across semiarid grasslands and shrublands [*Kurc and Small*, 2007]. Precipitation is balanced in the water budget by runoff, deep soil recharge, evapotranspiration (ET), and changes in soil water storage [*Huxman et al.*, 2005]. The partitioning of ET into plant transpiration, soil evaporation, and canopy-intercepted evaporation, while critical to the water budget, remains largely unknown due to limited observations [*Huxman et al.*, 2005; *Scott et al.*, 2006].

[5] The SWUS frequently experiences intense, prolonged droughts, such as the 1930s Dust Bowl (most intense in the American prairie), 1950s, and 1990s to 2000s. The most dramatic SWUS drought of the past 350 years, in terms of precipitation deficit, occurred in the 1950s [*McDonald*, 1956; *Schulman*, 1956], producing substantial die-off of lowland desert species, black grama, and upland conifer woodlands [*Herbel et al.*, 1972; *Swetnam and Betancourt*, 1998], with notable losses at the northern Chihuahuan sites of Sevilleta [*Betancourt et al.*, 1993] and Jornada Basin, NM [*Wright and Van Dyne*, 1976] (Figure 1). Since 1998, prolonged drought has produced serious regional water shortages [*Seager et al.*, 2007], shrub encroachment [*Van Auken*, 2000], greater wildfire risks [*Carter*, 2003; *Seager et al.*, 2007], and widespread tree mortality possibly exceeding that of the 1950s drought [*Ogle et al.*, 2000; *Breshears et al.*, 2005; *Shaw et al.*, 2005]. The SWUS may become increasingly hotter, drier in spring, and drought-prone during this century [*Christensen et al.*, 2007; *Seager et al.*, 2007], based on projections from the Fourth Assessment Report of the Intergovernmental Panel on Climate Change (IPCC AR4).

[6] Traditionally, the "pulse-reserve" conceptual paradigm states that annual net primary productivity (ANPP) in semiarid regions is linearly related to annual precipitation, with episodes of rainfall triggering pulses of plant growth [*Noy-Meir*, 1973]. However, this simplified model has been recently challenged for the Sonoran Desert by *Shen et al.* [2005], who argue that rainfall seasonality can determine plant growth, and for the northern Chihuahuan Desert by *Muldavin et al.* [2008], who suggest that cool season C3 plants respond instead to nonpulsed dynamics of accumulated winter soil moisture and the break of cold dormancy.

[7] The seasonal cycle of SWUS vegetation productivity, as represented by the normalized difference vegetation index (NDVI), is complex, with both unimodal and bimodal patterns observed temporally. Several studies have identified a bimodal seasonal cycle of vegetation growth in the northern Chihuahuan Desert, including the Sevilleta Long-Term Ecological Research (LTER) site [*Kemp*, 1983; *Weiss et al.*, 2004b; *Pennington and Collins*, 2007], but explanations vary among studies. One temperature-based theory attributes the dual peak to different optimum temperatures for photosynthesis, with C3 plants preferring lower temperatures typical of spring and C4 plants preferring higher temperatures during late summer [*Weiss et al.*, 2004b]. Another, moisture-based explanation is that C3 plants benefit from deep-water storage produced by winter-spring frontal systems, while C4 plants rely on late summer/early autumn monsoon rainfall [*Kemp*, 1983; *Pennington and Collins*, 2007]. A third, sunlight-based argument attributes the summertime NDVI minimum to surface litter loss from photodegradation [*Kremer and Running*, 1993; *Weiss et al.*, 2004a]; however, long-term accumulation and degradation may approach a steady state, putting this mechanism into question. All of these studies are site-specific, with no prior attempts at a regional-scale mechanistic modeling analysis.

[8] This paper addresses the following questions: (1) What are the mechanisms by which climate, soil moisture, snow cover, vegetation, and ET interact across various SWUS ecosystems? (2) What are the reasons for unimodal versus bimodal seasonal cycles of productivity and where are they found in the SWUS? Unlike previous site-specific ecological studies, this study explores the spatial variability of the seasonal cycle of vegetation productivity, soil moisture, and evaporation across diverse SWUS ecosystems, using a wide array of data sets and simulations. The analysis exploits an expanded 25 year series of remotely sensed

Table 1. Summary of Data Sets, Including Variables, Resolution or Sites, Period, and Sources/References

Data Set	Variables	Resolution/Sites	Period	Sources or References
Climatic Research Unit Time Series Version 2.1 (CRU TS2.1)	Monthly temperature, precipitation, cloud cover, number of wet days	0.5° × 0.5° global	1901–2002	*Mitchell and Jones* [2005]
University of Delaware (WM)	Monthly temperature, precipitation	0.5° × 0.5° global	1901–2006	*Willmott and Matsuura* [1995]
NASA MODIS ET data set	8 day composite ET estimates, from satellite data and Penman-Monteith equation [*Monteith*, 1964]	0.05° × 0.05° global	2000–2006	*Cleugh et al.* [2007], *Mu et al.* [2007a, 2007b]
NOAA CPC Evaporation data set	Monthly evaporation simulated by hydrologic model with temperature and precipitation input	344 U.S. climate divisions	1932–2006	*Huang et al.* [1996], *van den Dool et al.* [2003]
University of Delaware's Willmott-Matsuura Terrestrial Water Budget Time Series	Monthly ET estimates using *Willmott et al.*'s [1985] modified Thornthwaite water budget	0.5° × 0.5° global	1950–1999	climate.geog.udel.edu/~climate/html_pages/README.wb_ts2.html
Variable Infiltration Capacity (VIC) Retrospective Land Surface data set	Monthly evaporation from macroscale hydrologic model, forced by observed meteorological data	1/8° × 1/8° U.S.	1950–2000	*Maurer et al.* [2002]
North American Regional Reanalysis (NARR) Evaporation data set	Daily evaporation from NARR, using NCEP Eta Model coupled to NOAH Land Surface Model with Regional Data Assimilation System	32 km North America	2000–2006	www.cdc.noaa.gov/cdc/data.narr.html, *Mesinger et al.* [2006], *Chen et al.* [1997]
Ameriflux data set	Half-hourly latent heat flux	Niwot Ridge, CO; Audubon, AZ	1999–2006, 2003–2006	public.ornl.gov/ameriflux
Sevilleta LTER	Half-hourly latent heat flux	Sevilleta, NM	2007–2008	University of New Mexico
Figure 3 of *Mielnick et al.* [2005]	Monthly ET	Jornada Basin, NM	1996–2001	*Mielnick et al.* [2005]
Ivans et al. [2006] data	Daily ET, near Payson	Rush Valley, UT	2002–2003	*Ivans et al.* [2006]
Ameriflux/LTER data set	Half-hourly soil moisture at 0–15 cm	Niwot Ridge, CO	2002–2007	spot.colorado.edu/~monsonr
Ameriflux data set	Half-hourly soil moisture at 5, 10 cm	Audubon, AZ	2002–2006	ftp://cdiac.ornl.gov/pub/ameriflux
NPP Soil Water Content LTER data set	Monthly soil moisture at 30, 120 cm	Jornada Basin, NM	1990–2006	jornada-www.nmsu.edu
NSF-funded Sevilleta LTER data set	Hourly soil moisture at 5, 20, 40 cm	Sevilleta, NM	1996–2001	sev.lternet.edu
Snowpack Telemetry (SNOTEL)	Hourly/daily soil moisture at 5, 20, 50 cm: Baldy, Happy Jack, AZ; Camp Jackson, Little Grassy, Payson, Temple Fork, UT	2 AZ sites; 4 UT sites	2002–2008; 2003–2006	USDA
Global Continuous Fields of Vegetation Cover (GCFVC): International Satellite Land Surface Climatology Project (ISLSCP2)	Tree, herbaceous, deciduous tree, evergreen tree cover fractions, based on Advanced Very High Resolution Radiometer NDVI	0.5° × 0.5° global	Snapshot	*DeFries et al.* [1999, 2000a, 2000b]
EROS Data Center (EDC) Land Cover data set from ISLSCP2	Geographic distribution of 17 land cover classes	0.25° × 0.25° global	Snapshot	*Loveland and Belward* [1997], *Loveland et al.* [2001]
ISLSCP2 C4 Vegetation Percentage	Percent C4 plant cover, based on C4 climate classification map, GCFVC data set, crop and harvest area	1° × 1° global	Snapshot	*Still et al.* [2003]

Table 1. (continued)

Data Set	Variables	Resolution/Sites	Period	Sources or References
Figure 1 and Appendix Table 1 from *Paruelo and Lauenroth* [1996]	Relative abundance of C3/C4 grasses and mean temperature/precipitation	23 SWUS sites	Snapshot	*Paruelo and Lauenroth* [1996]
Potential Natural Vegetation (PNV)	Natural distribution of 15 vegetation types	5′ and 0.5° global	Snapshot	*Ramankutty and Foley* [1999]
GIMMS NDVI	2 week NDVI composites, corrected for stratospheric aerosol and satellite drift	8 km and 0.5° global	1982–2006	*Tanre et al.* [1992], *Pinzon et al.* [2004]
Long-Term Ecological Research (LTER) Plant Phenology Transects (NSF funded)	Weekly/monthly status of plant phenological events (e.g., budding, flowering, fruiting)	Sevilleta, NM; Jornada Basin, NM	1991–1995; 1993–2004	*Gosz* [1994]; *Huenneke and Peters* [1992]

NDVI, vital for characterizing unimodal versus bimodal seasonal cycles, and a new satellite-based method for estimating ET [*Cleugh et al.*, 2007; *Mu et al.*, 2007a, 2007b], in addition to ecohydrology data sets from multiple sites, to address the spatiotemporal complexity of ecohydrological processes across the SWUS. By applying a dynamic vegetation model that is adapted to the SWUS, a deeper understanding of the region's ecohydrology [*Vivoni et al.*, 2010] is sought.

2. Materials and Methods

2.1. Data

[9] Table 1 summarizes the data sets used in this study. The driving fields for LPJ include two 0.5° × 0.5° observation-based gridded global climate data sets: the Climatic Research Unit Time Series Version 2.1 (CRU TS2.1) data set and University of Delaware's Willmott-Matsuura (WM) data set. Both include monthly air temperature and precipitation, while the former also contains monthly cloud cover and wet day frequency.

[10] Several site-level data sets, from Ameriflux, LTER, SNOTEL (Snowpack Telemetry), *Mielnick et al.* [2005], and *Ivans et al.* [2006] are analyzed to understand the seasonal cycle of ET and soil moisture. Also analyzed is the NASA MODIS ET data set, based on the Penman-Monteith equation [*Monteith*, 1964] with daily meteorological inputs and remotely sensed data (method in auxiliary material).[1] These ET data sets are supplemented with regional estimates from the University of Delaware's Willmott-Matsuura Terrestrial Water Budget, NOAA Climate Prediction Center's (CPC) hydrological model, Variable Infiltration Capacity (VIC) hydrological model, and the North American Regional Reanalysis (NARR).

[11] Several data sets are used to determine regional vegetation characteristics, including Global Continuous Fields of Vegetation Cover (GCFVC), EROS Data Center (EDC) Land Cover, International Satellite Land Surface Climatology Project (ISLSCP2) C4 Vegetation Percentage, *Paruelo and Lauenroth*'s [1996] site data on C3/C4 grass abundance and climate, and Potential Natural Vegetation (PNV). The vegetation model is evaluated and the seasonal cycle of vegetation greenness is studied using GIMMS NDVI for 1982–2006. NDVI is computed from the near-infrared (NIR) and red (RED) reflectance as follows:

$$NDVI = \frac{(NIR - RED)}{(NIR + RED)}.$$

[12] NDVI has a strong linear relationship with FPAR (fraction of photosynthetically active radiation, used to drive photosynthesis) [*Myneni et al.*, 1995; *Sellers*, 1985] and is related to biophysical variables (e.g., leaf area) and vegetation phenology [*Justice et al.*, 1985; *Spanner et al.*, 1990; *Prince et al.*, 1995]. The LTER Plant Phenology Transects data set from Sevilleta and Jornada Basin is used to relate satellite-based findings to surface observations.

[1] Auxiliary materials are available in the HTML. doi:10.1029/2010JG001382.

2.2. Implementation of the Vegetation Model

[13] To investigate the seasonal cycle of plant phenology, soil moisture, and evaporative fluxes in the SWUS, we apply the Lund-Potsdam-Jena Dynamic Global Vegetation Model (LPJ-DGVM) [*Sitch et al.*, 2003; *Gerten et al.*, 2004], which represents vegetation dynamics, carbon cycling, and water cycling processes. Vegetation is represented by 10 plant functional types (PFTs), including eight woody plants, C3 grasses, and C4 grasses. LPJ does not simulate shrubs but rather short trees. LPJ successfully simulates the mean global vegetation distribution [*Sitch et al.*, 2003], interannual vegetation responses to climate variability [*Lucht et al.*, 2002], global fire patterns [*Thonicke et al.*, 2001], and key hydrologic variables, including runoff, ET, and soil moisture [*Sitch et al.*, 2003; *Wagner et al.*, 2003; *Gerten et al.*, 2004]. LPJ contains a 0.5 m upper soil layer, with an embedded 20 cm surface evaporative layer, and a lower 1 m soil layer.

[14] In LPJ, the net simulated foliar projective cover, or FPC, is computed as a function of crown area, the number of individuals, and the mean leaf area of the average individual. Using annual vegetation cover fractions, or FPC, and daily leaf cover (phenology) fractions (DPHEN) for each PFT, FPAR is computed as follows [*Sitch et al.*, 2000]:

$$FPAR = \sum_{pft=1}^{10} FPC_{pft} * DPHEN_{pft}.$$

When converting simulated FPAR into NDVI for comparison with satellite NDVI, we apply this empirical linear relationship from *Ruimy et al.* [1994], based on global remotely sensed data:

$$NDVI = \frac{FPAR + 0.025}{1.25}.$$

This equation, based on the linearity of the NDVI-FPAR relationship [*Hall et al.*, 1992; *Myneni and Williams*, 1994; *Myneni et al.*, 1997; *Fensholt et al.*, 2004], is consistent with empirical formulas from *Baret and Olioso* [1989], *Asrar et al.* [1984], and *Daughtry* [1988].

[15] LPJ is run on a 0.5° × 0.5° grid across 31°N–42°N, 115°W–102°W (Figure 1), for 1901–2006, forced by monthly temperature, precipitation, cloud cover, and wet day frequency. LPJ linearly interpolates monthly temperatures to daily and uses the number of wet days to randomly distribute monthly precipitation into daily events of varying intensity. Thus, the size distribution and frequency of precipitation events, which differ dramatically between winter and summer, are accounted for in the simulations. The auxiliary material contains details on LPJ processes, input data, regional adaptations, and performance. The simulation begins with a 1000 year spin-up from bare ground to allow land carbon pools to reach equilibrium [*Sitch et al.*, 2003], forced by a repeated cycling of 1901–1930 climate data which includes both wet and dry years. This represents the "control simulation", against which sensitivity experiments are later compared.

[16] While LPJ produces a reasonable global vegetation distribution, it is unlikely that a global model would necessarily display high accuracy in a regional simulation without regionally specific adaptations. Four key simulation biases are identified across the SWUS: vegetation cover is overproduced, especially grass; no C4 grasses are simulated; too little forest cover is produced at higher elevations in Arizona; and deciduous tree cover is under simulated. Several SWUS-specific adjustments are made to the model and input data, which reduce these biases (detailed in auxiliary material). A new soil data set, with a better representation of coarse soil types in Arizona and New Mexico, is applied. The specific leaf areas for grasses and needleleaf evergreen trees and the establishment rate of evergreen trees are reduced, based on measurements. The required growing degree days (GDDs) for summer phenology vegetation to achieve full leaf canopy is increased, while applying a ramp factor that makes senescence more gradual. The boreal heat stress term is removed. New temperature criteria are applied to separate C3 from C4 grasses. The 20 year maximum coldest month temperature for temperate broadleaf summergreen trees is reduced to represent winter chill requirements, while decreasing the minimum 20 year GDDs for boreal needleleaf evergreens to simulate high-elevation forests.

[17] The regionally adapted version of LPJ produces both mean and time-varying patterns in vegetation cover fraction that agree reasonably with satellite data during 1982–2000, along with substantial vegetation die-offs in response to the droughts of the 1930s, 1950s, and 1990s to 2000s (auxiliary material). The model, however, produces exaggerated vegetation die-offs during droughts, which is explored in section 4. Although simulated results are compared with observations in the paper, a perfect match should not be expected since this version of LPJ simulates only natural vegetation, without considering human activities (e.g., deforestation, grazing, crops, human-induced or suppressed fires).

2.3. Sensitivity Experiments

[18] Given that model experiments are the only viable method to test the pulse-reserve hypothesis on a regional scale, we perform a series of LPJ sensitivity experiments focused on the impact of snowmelt, soil moisture, transpiration, precipitation, and temperature on the seasonal cycle of NDVI in the SWUS.

[19] 1. In order to assess the importance of snowmelt for supplying a springtime surge of soil moisture for plant growth, experiment EXP_SNOW is performed in which the snowpack is allowed to melt but the meltwater does not enter the soil.

[20] 2. The influence of soil moisture and drought response on the seasonal cycle of NDVI is investigated by a pair of experiments, EXP_SOIL. Drought deciduous PFTs, including grasses, shed their leaves or become phenologically inactive when the computed water scalar value, representing total available soil moisture and ranging from 0 (dry) to 1 (wet), falls below a specified value, which is by default 0.1. Over the SWUS, this represents grasses wilting during periods of dry soil. The 1901–2006 simulation is repeated twice, using water scalar criteria of 0.0 (implying that grasses never wilt due to low soil moisture) and 0.2 (implying that grasses are more sensitive to low soil moisture).

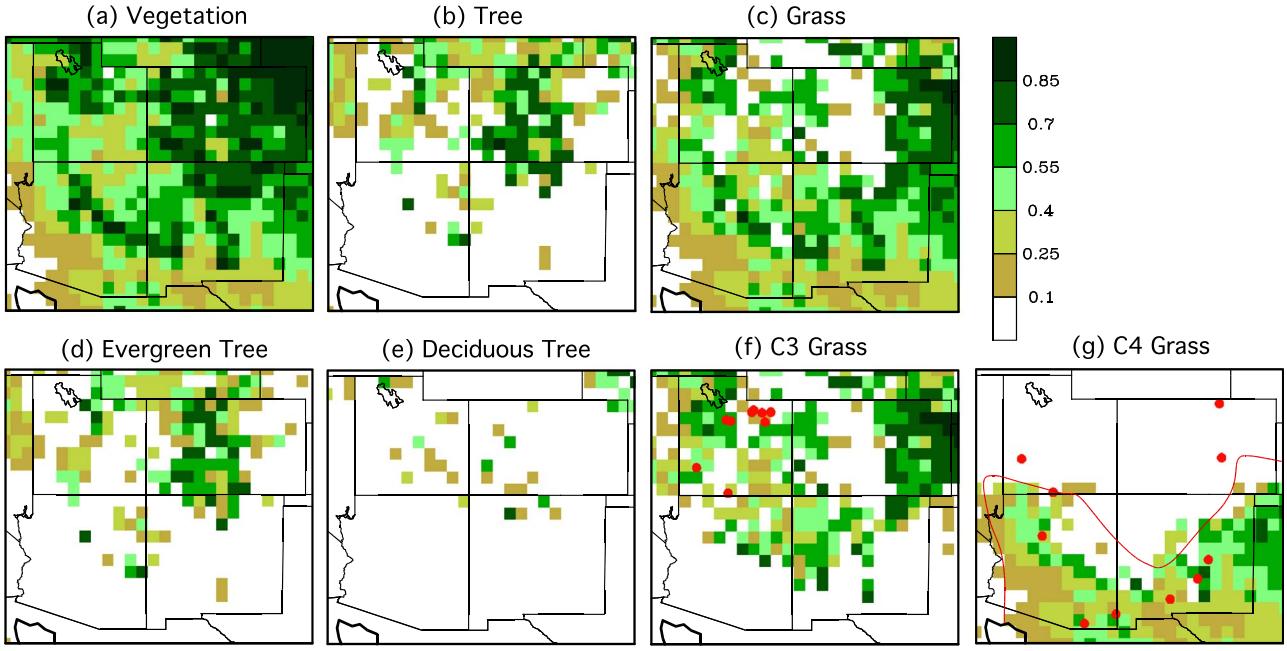

Figure 2. Simulated fractional cover, averaged over 1901–2006, of (a) vegetation (tree plus grass), (b) tree, (c) grass, (d) evergreen tree, (e) deciduous tree, (f) C3 grass, and (g) C4 grass. The red dots indicate the location of sites reported by *Paruelo and Lauenroth* [1996] to be dominated by C3 grasses (Figure 2f) or C4 grasses (Figure 2g). The red line in Figure 2g is the approximate boundary between primarily C3 plants to the north and primarily C4 plants to the south, from the ISLSCP2 C4 Vegetation Percentage data set.

[21] 3. To assess the influence of precipitation seasonality on NDVI seasonality, experiment EXP_PREC is performed in which the seasonal cycles of monthly precipitation amount and frequency during 1982–2006 are replaced by their annual mean values.

[22] 4. In order to investigate the impact of warming from climate change on the seasonal cycle of SWUS vegetation (e.g., distribution of areas with a bimodal NDVI seasonal cycle), the 1901–2006 simulation is repeated as EXP_TEMP with a uniform temperature increase of 5°C, reflecting the predicted 21st century SWUS warming in the A2 scenario of IPCC AR4.

[23] 5. In EXP_TRANSP, plant transpiration may not exceed 0.3 mm/d during March–June, so that the impact of transpiration during the initial springtime NDVI surge can be assessed.

3. Results

3.1. Spatial Distribution of Vegetation

[24] Total simulated vegetation cover, averaging 0.52, is partitioned into 0.15 for trees (evergreen = 0.12, deciduous = 0.03) and 0.37 for grasses (C3 = 0.22, C4 = 0.15) (Figure 2). LPJ produces a reasonable PFT distribution compared to EROS, PNV, and GCFVC data sets. Evergreen forests dominate at higher elevations in western Colorado, northeastern Utah, and central Arizona (Figure 2d). Pockets of deciduous forests are simulated in eastern Utah and western Colorado (Figure 2e) where early successional quaking aspens are observed [*Baker*, 1925; *Brown*, 1935; *Day*, 1944]. LPJ produces too little high-elevation evergreen forests in Arizona and New Mexico, as the use of coarse resolution climate data causes LPJ to miss PFTs that occupy small spatial climate niches [*O'Brien*, 2002; *Arora and Boer*, 2006]. In agreement with *Paruelo and Lauenroth* [1996] and C4 ISLSCP2 data sets, simulated C3 grasses dominate in the cooler northern domain (Figure 2f), while C4 grasses persist in the warmer southern domain (Figure 2g). LPJ produces too much C3 grasses in eastern Colorado (Figure 2f). Low vegetation cover is simulated and observed over the Sonoran, Chihuahuan, Mojave, and Great Basin Deserts and Colorado Plateau (Figures 1 and 2).

[25] Observed and simulated annual NDVI peak over evergreen forests in western Colorado, central Utah, and central Arizona and grasslands in eastern Colorado and eastern New Mexico, while both are low over the Sonoran, Chihuahuan, Mojave, and Great Basin Deserts and Colorado Plateau (Figures 3a and 3f). The area-averaged annual NDVI in the observations and model is 0.25 and 0.30, respectively. The simulated area-averaged NDVI differs from satellite values by −0.02 in JFM to +0.13 in JAS; a perfect match is not expected since LPJ only simulates natural vegetation. Ranching and grazing have reduced vegetation cover, while fire suppression has favored scattered shrubs rather than widespread grasses. Unlike the model, during winter, satellite NDVI in the absence of vegetation does not drop to zero due to false signals from bare soil [*Kremer and Running*, 1993; *Peters and Eve*, 1995] (Figures 3b and 3g). The spatial correlation between annual observed and simulated NDVI is 0.63 ($p < 0.01$, N = 672 grid cells). Potential biases in the empirical regression formula for converting simulated FPAR into NDVI could

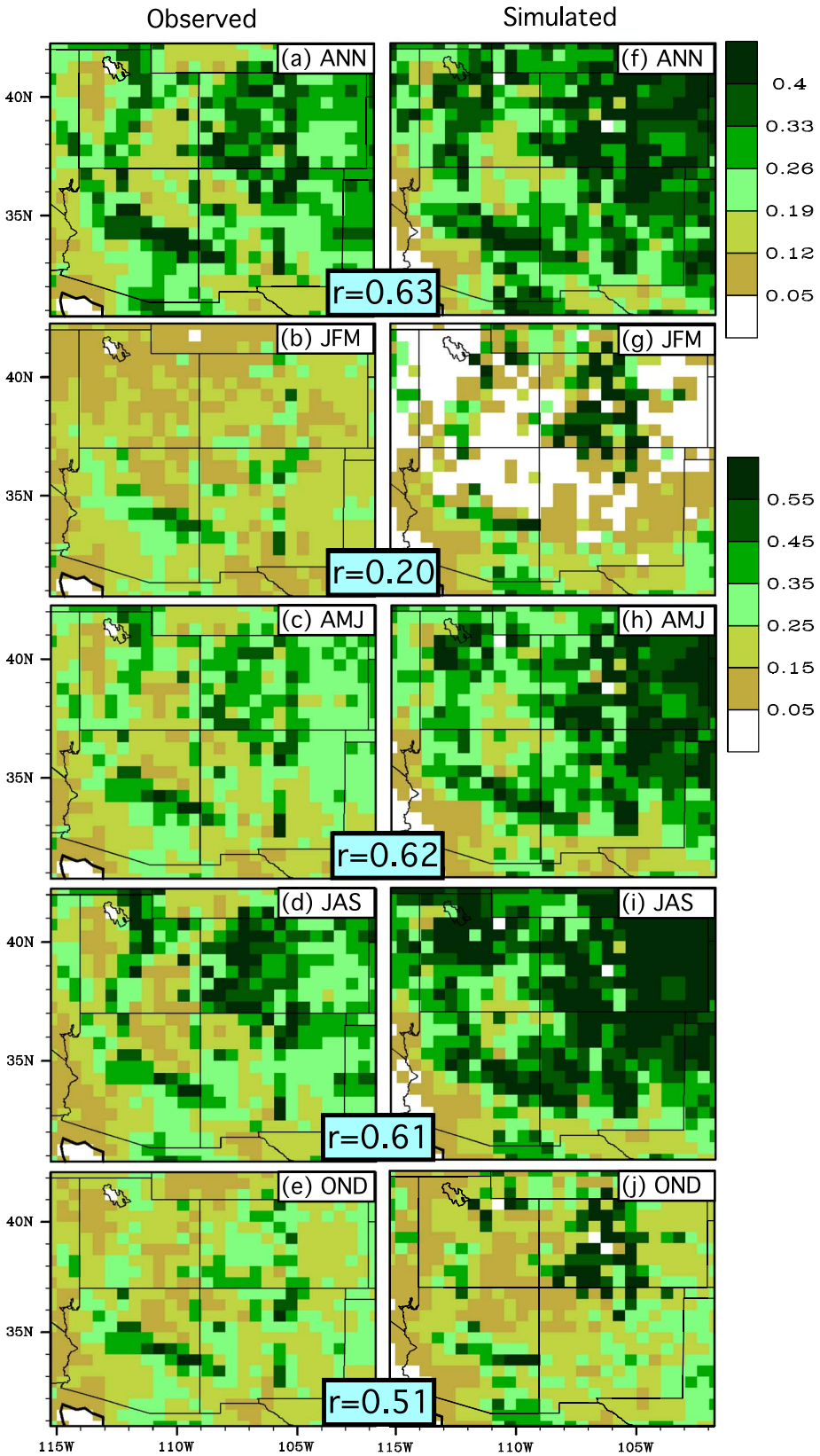

Figure 3. Mean (a–e) GIMMS satellite and (f–j) simulated NDVI for 1982–2006, both annually (top color bar) and by season (bottom color bar). Since the monsoon over the SWUS occurs during JAS, we chose to display the seasons of JFM, AMJ, JAS, and OND, rather than the climatological seasons (e.g., JJA). In each blue box, the spatial correlation between satellite and simulated NDVI for each season is displayed (N = 672 grid cells).

Table 2. Summary of 10 Sites Analyzed in the Study[a]

		Observed Biome		DeFries Data			Mean Climate			Mean NDVI		Mean Soil Water[b]		Model Mean Vegetation					
Site	Coordinates	PNV	EROS	Herbaceous	Deciduous	Evergreen	T (°C)	P (mm/month)	GDD	Observed	Model	Observed	Model	Tree	Grass	Deciduous	Evergreen	C3 Grass	C4 Grass
Niwot Ridge, Colorado (NIW)	40.02°N, 105.53°W	Evergreen forest, grassland	Woody savanna	0.58	0.12	0.28	3.9	36.4	1050	0.47	0.43	0.17, X	0.17, 0.19	0.39	0.27	0.00	0.39	0.27	0.00
Baldy, Arizona (BAL)	33.97°N, 109.50°W	Evergreen forest, shrubland	Woody savanna, evergreen forest	0.70	0.05	0.21	9.2	38.2	2130	0.44	0.49	0.16, 0.08	0.20, 0.21	0.43	0.30	0.00	0.43	0.19	0.10
Temple Fork, Utah (TEM)	41.78°N, 111.53°W	Deciduous forest, shrubland	Deciduous forest, grassland	0.74	0.07	0.18	7.9	41.9	1700	0.35	0.34	0.21, 0.18	0.24, 0.24	0.26	0.67	0.25	0.00	0.67	0.00
Happy Jack, Arizona (HAP)	34.73°N, 111.40°W	Evergreen forest, shrubland	Evergreen forest	0.72	0.02	0.17	14.3	40.1	3510	0.46	0.39	0.24, 0.24	0.26, 0.25	0.05	0.54	0.00	0.05	0.18	0.36
Payson, Utah (PAY)	39.92°N, 111.62°W	Grassland, mixed forest	Grassland, deciduous forest	0.85	0.12	0.02	7.7	30.7	1740	0.34	0.36	0.20, 0.24	0.18, 0.20	0.14	0.68	0.04	0.11	0.68	0.00
Sevilleta, New Mexico (SEV)	34.35°N, 106.88°W	Shrubland	Shrubland	0.80	0.00	0.00	12.4	24.6	2610	0.18	0.28	0.10, X	0.08, 0.07	0.01	0.56	0.00	0.01	0.17	0.39
Jornada Basin, New Mexico (JOR)	32.62°N, 106.74°W	Shrubland	Shrubland	0.74	0.00	0.00	16.1	19.9	3840	0.17	0.24	0.09, 0.10	0.11, 0.11	0.00	0.35	0.00	0.00	0.00	0.35
Audubon, Arizona (AUD)	31.59°N, 110.51°W	Grassland, shrubland	Woody savanna, deciduous forest	0.89	0.02	0.05	17.2	29.6	4110	0.30	0.37	0.16, X	0.07, 0.07	0.00	0.46	0.00	0.00	0.00	0.46
Little Grassy, Utah (LIT)	37.48°N, 113.83°W	Shrubland	Grassland, woody savanna	0.77	0.01	0.08	10.3	24.2	2140	0.36	0.24	0.15, 0.11	0.18, 0.21	0.02	0.51	0.00	0.02	0.51	0.00
Camp Jackson, Utah (CAM)	37.80°N, 109.48°W	Grassland, evergreen forest	Grassland	0.83	0.06	0.04	9.3	26.3	2310	0.37	0.28	0.22, 0.20	0.21, 0.23	0.21	0.31	0.07	0.14	0.31	0.0

[a]The first five sites are generally forested, and the last five are generally grassland-shrubland. For each site, the following information is provided: geographical coordinates in °N, °W; observed biome (PNV, EROS); fractional cover from DeFries' GCFVC data (herbaceous, deciduous tree, evergreen tree); annual mean climate (temperature (°C), precipitation (mm/month), growing degree days base 5°C); annual mean NDVI (GIMMS, LPJ); mean upper and lower soil water content fraction (observed, LPJ); and simulated vegetation cover fractions (tree, grass, deciduous tree, evergreen tree, C3 grass, C4 grass). For sites where sufficient data on observed soil water fraction is not available, an "X" is shown.

[b]Format is upper, lower.

contribute toward some of the differences between remotely sensed and modeled vegetation.

[26] NDVI peaks in a clockwise map pattern across the SWUS (Figures 3 and 9a), beginning in spring in the Sonoran Desert following winter rains, then in Utah and Colorado with snowmelt/summer rains, and finally in New Mexico–eastern Arizona with late summer-autumn monsoon rains. The SWUS area average NDVI peaks in June–September in the model and observations, although LPJ simulates too much leaf cover during the growing season. High NDVI values are simulated year-round in the high-elevation evergreen forests (Figures 3g–3j). This is generally true of the

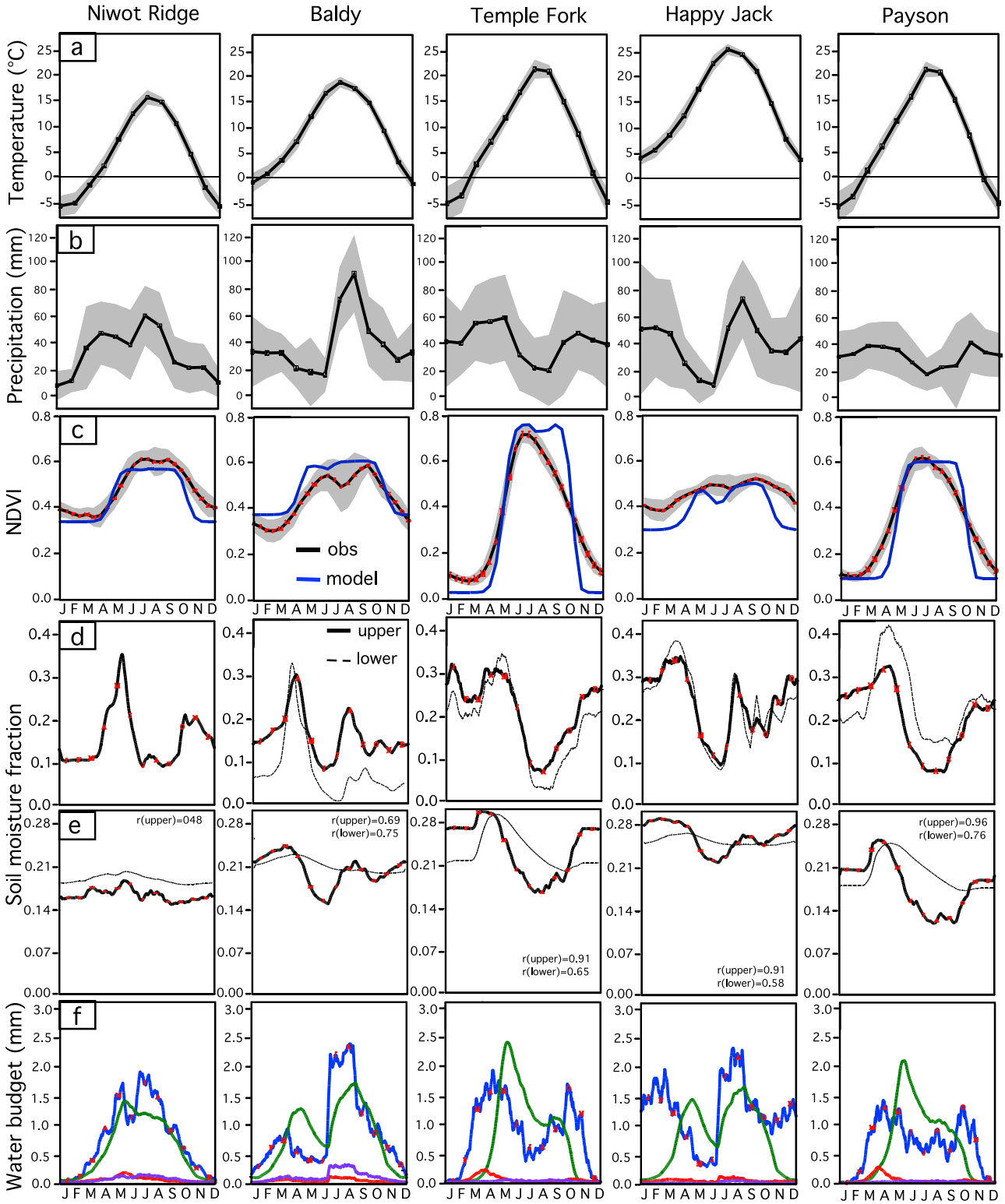

Figure 4

observed NDVI except high cold-season NDVI values are not detected over Utah and Colorado due to false signals from snow [*Reed and Sayler*, 1998] (Figures 3b–3e).

[27] The seasonal cycles of climate, vegetation greenness, soil moisture, and evaporation (Table 2 and Figures 4 and 5) are analyzed at 10 SWUS sites (Figure 1), which have extensive observations through Ameriflux, LTER, and SNOTEL and represent a variety of SWUS ecosystems. While most prior studies have focused on individual sites, such as Sevilleta [*Weiss et al.*, 2004a, 2004b]; Jornada Basin [*Wright and Van Dyne*, 1976]; Niwot Ridge, CO [*Isard*, 1986]; Happy Jack, AZ [*Hawkins and Ellis*, 2007]; and Audubon, AZ [*Xiao et al.*, 2008], we have performed a comprehensive, region-wide analysis of soil-vegetation-atmosphere interactions.

[28] The first five sites in Table 2 are generally high-elevation, forested locations, while the last five are better described as grasslands-shrublands. Mean precipitation is greater at the forested sites (Table 2, fifth column). The monsoon influences rainfall most notably at the four southernmost sites (Audubon; Jornada Basin; Sevilleta; and Baldy, AZ), with a prominent July–August unimodal rainfall peak (Figures 4b and 5b). Seasonal precipitation is distinctly bimodal at the remaining six, northernmost sites, typically including winter-spring and summer-autumn peaks (Figures 4b and 5b). There is a sharp contrast in mean annual temperature, ranging from 3.9°C at Niwot Ridge to 17.2°C at Audubon (Table 2, fifth column). While vegetation across much of the SWUS is water limited, temperature also plays a crucial role in controlling plant growth, particularly in frost-prone regions at high elevations and regions with large seasonal or diurnal temperature cycles.

[29] Based on EROS, PNV, and GCFVC data sets, the representative biome of Niwot Ridge, Baldy, and Happy Jack is evergreen forest, of Temple Fork is deciduous forest, and of Payson is deciduous forest-grassland (Table 2, third and fourth columns). LPJ generally simulates the same categories for these sites but produces mostly grasses at Happy Jack (Table 2, eighth column). Sevilleta and Jornada Basin are mostly shrublands, while Audubon; Little Grassy, UT; and Camp Jackson, UT are within grasslands/savannas (Table 2, third and fourth columns). LPJ simulates grasslands in Sevilleta, Jornada Basin, Audubon, and Little Grassy and grass-forest mix in Camp Jackson (Table 2, eighth column), thus approximating observations. Prior to anthropogenically induced twentieth century shrub encroachment, the northern Chihuahuan Desert (e.g., Jornada Basin and Sevilleta) was largely a lush, warm-season C4 grassland with greater vegetation cover than at present [*Cornelius et al.*, 1991; *Tweit*, 1995; *Reynolds et al.*, 2000; *Laliberte et al.*, 2004], making grass its natural vegetation type. The higher productivity at northern Chihuahuan Desert sites simulated by LPJ relative to satellite data, along with the simulated dominance of grasses at these sites, suggests that LPJ is correctly capturing the natural vegetation. At the northern sites in Utah and Colorado, LPJ accurately represents the success of C3 over C4 grasses (Table 2, eighth column, and Figure 2g). Simulated grass types are limited to C4 at the southernmost sites of Jornada Basin and Audubon, while both types coexist at Baldy, Happy Jack, and Sevilleta in central Arizona–New Mexico (Table 2, eighth column). Sevilleta grasslands are primarily C4 at present, with some C3 cover observed during spring.

[30] The correlation between annual mean NDVI at the 10 sites from LPJ and the GIMMS satellite data is 0.70 ($p < 0.05$); the model has no mean bias and is generally within ± 0.06 of the observations (Table 2, sixth column). Annual mean NDVI, from both GIMMS and LPJ, is largest at the evergreen sites of Niwot Ridge, Baldy, and Happy Jack. The lowest annual mean NDVI is observed at the northern Chihuahuan Desert sites of Jornada Basin and Sevilleta, due to limited rainfall and coarse soil.

[31] A consistent relationship is apparent in the observations and model between annual precipitation and upper soil water fraction ($r = 0.67$, $p < 0.05$), with both variables highest at Temple Fork and Happy Jack and lowest at Jornada Basin, Sevilleta, and Little Grassy (Table 2, fifth and seventh columns). There is a strong relationship between observed annual upper soil water fraction and NDVI, with the least upper soil water and vegetation amount at Jornada Basin and Sevilleta (Table 2, sixth and seventh columns). The forested sites have an observed mean upper soil water fraction that is 0.05 higher than grassland/shrubland sites. The simulated upper soil water fraction is well correlated with ($r = 0.81$, $p < 0.01$), and generally within ± 0.03 of, site observations (Table 2, seventh column). The simulated lower soil water fraction is generally too high but within ± 0.05 of observed; allowing soil types to vary by depth, or increasing the drainage, might improve this deficiency.

3.2. Annual Cycle: Vegetation

[32] The SWUS is characterized by a complex seasonal cycle of vegetation productivity (Figures 4c and 5c). The seasonal evolution of NDVI reflects the reactivation of

Figure 4. Mean seasonal cycle for Niwot Ridge, Baldy, Temple Fork, Happy Jack, and Payson. Variables include (a) temperature ("Temp", °C) and (b) precipitation ("Prec", mm/month) from the observational WM data set, (c) GIMMS (black, based on several pixels for each site) and simulated (blue) NDVI, (d) observed upper (solid) and lower (dashed) volumetric soil moisture fraction, (e) simulated upper (solid) and lower (dashed) volumetric soil moisture fraction ("Soil M"), and (f) simulated water budget (mm/d) (blue, effective rainfall ("prec", not including snowfall or intercepted precipitation); green, transpiration ("trans"); red, bare soil evaporation ("bare"); purple, canopy intercepted evaporation ("interc")). Time periods for computing the averages are 1982–2006 for Figures 4a–4c and 1901–2006 for Figure 4f, while the periods in Figures 4d and 4e varied by site depending on available observations. The gray shading in Figures 4a–4c indicates the interannual standard deviation of monthly temperature (Figure 4a), precipitation (Figure 4b), and satellite NDVI (Figure 4c). The horizontal lines in Figure 4a indicate 0°C. Upper (lower) soil water fraction is computed by averaging observed level measurements taken within 0–40 cm (50–120 cm) depth and compared to the model's upper (lower) soil layer average at 0–50 cm (50–150 cm) depth. Temporal correlations (N = 365 days) between observed and simulated (upper and lower) soil moisture fractions are shown in Figure 4e.

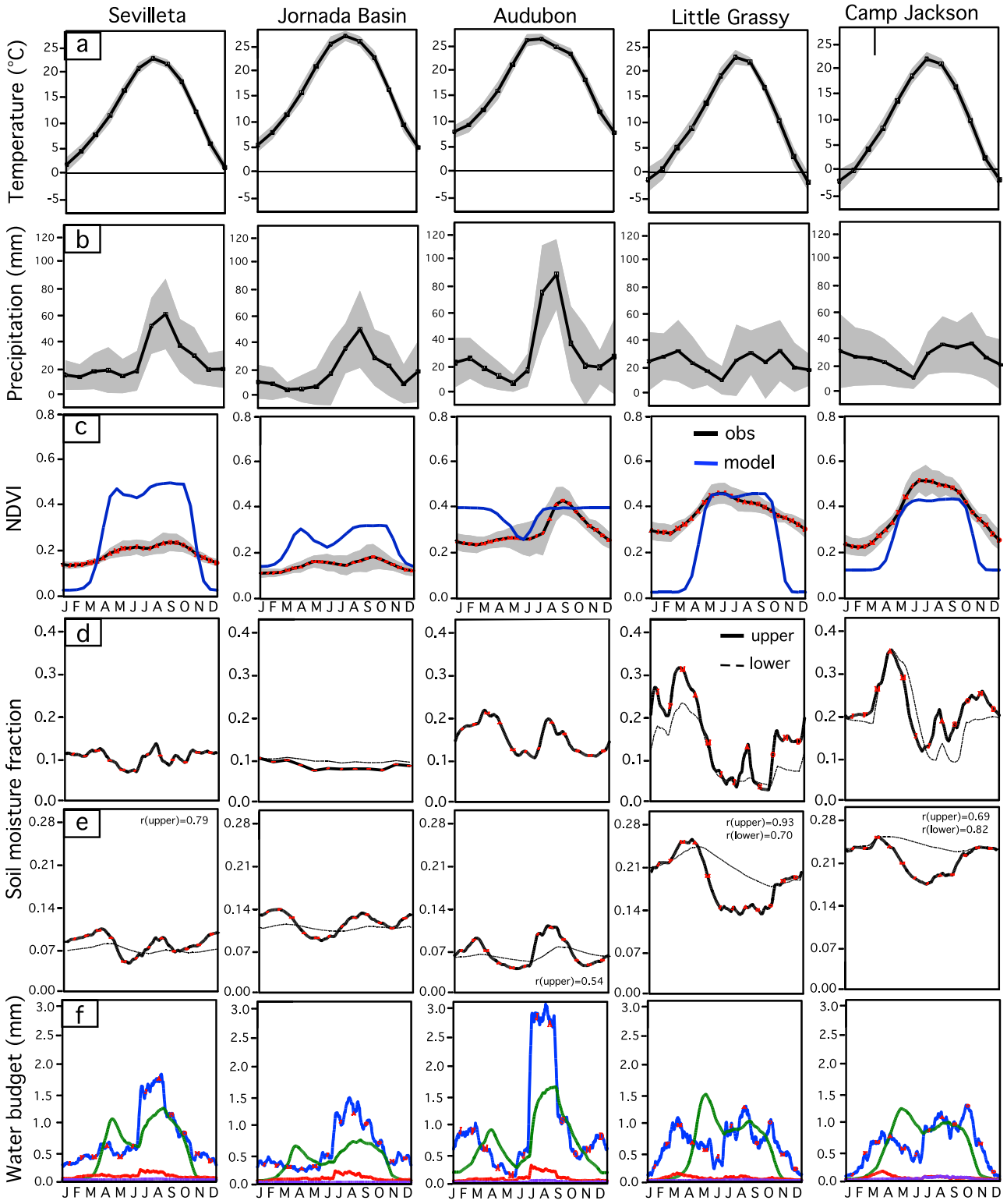

Figure 5. Same as Figure 4, except for Sevilleta, Jornada Basin, Audubon, Little Grassy, and Camp Jackson.

green-up and the emergence of different seasonal species. Observed NDVI peaks in June–July for the Utah-Colorado sites and September for the Arizona–New Mexico sites. While much of the region is characterized by a unimodal NDVI peak, a bimodal NDVI seasonal cycle is evident at Baldy and Happy Jack, AZ and Sevilleta and Jornada Basin, NM, with a late spring–early summer initial peak, a middle to late summer dip, and a second peak in autumn. Across the northern Chihuahuan Desert, the semievergreen C3 creosotebush and many annuals are active in springtime in

response to accumulated wintertime deep soil moisture. The late summer monsoon green-up consists mostly of blue and black grama, or C4 grasses, benefiting from abundant shallow soil moisture. The dependence of greening at the North American monsoon sites on monsoon rainfall, along with the 1 month lag between August monsoon rainfall and peak green-up in September are in agreement with findings of *Lizárraga-Celaya et al.* [2010] and *Vivoni et al.* [2008]. Despite significant discrepancies between observed and simulated NDVI seasonal cycles, the model successfully simulates a dual peak in vegetation abundance at the aforementioned four sites, although the timing of maxima and minima is sometimes shifted. The interannual variability in observed NDVI is greatest in May–June for the northernmost sites, following the highly variable springtime snowmelt, and in August–September for the New Mexico sites, related to monsoon rainfall variability. In exceptionally warm regions (e.g., Audubon), LPJ incorrectly simulates active grasses throughout winter due to sufficient warmth, underestimating precipitation's control on vegetation growth.

[33] While the Utah/Colorado sites and Audubon exhibit a unimodal NDVI seasonal cycle, the mechanisms are quite different. At the Utah/Colorado sites, springtime snowmelt and an initial precipitation peak support springtime plant emergence, with 3–4 months of gradual plant growth until the summertime NDVI peak. At Audubon, an initial late winter–early spring soil moisture peak, resulting from wintertime precipitation events, does little to support plant growth, as the C4 grasses in that region prefer higher temperatures. The summertime monsoon provides the moisture for a rapidly established (over 1–2 months) September NDVI maximum.

3.3. Annual Cycle: Soil Moisture

[34] The mean seasonal cycle of soil water fraction is analyzed from observations and LPJ (Figures 4d, 4e, 5d, and 5e). All sites exhibit observed maxima in upper and lower soil water fraction in March–May, related to spring snowmelt at colder sites (Figure 5d of *Hamlet et al.* [2007]) and soil moisture accumulation from modest winter precipitation and limited cool-season transpiration loss due to inactive vegetation. For the northernmost sites, a spring precipitation pulse augments the sizable April–May snowmelt in supplying ample soil moisture. The five southernmost sites, in Arizona and New Mexico, display relative maxima in observed soil moisture during July–August related to monsoon rainfall, which recharges soil moisture following a hot, dry late spring–early summer. All Utah sites exhibit a second precipitation peak in October, enhancing soil moisture observed in October–December. LPJ accurately simulates the timing of the seasonal cycle, but not always the amount, of upper and lower soil moisture at the 10 sites. Differences between observed and simulated soil moisture could be due to model biases, comparison of observed moisture at specified levels to simulated layer-averaged moisture in a grid cell, differences in observed and modeled soil composition, or measurement errors.

[35] Due to limited soil moisture measurements, the number of years analyzed at each site ranges from only 4 to 17 years (Figures 4d, 4e, 5d, and 5e), shorter than preferred for a stable climatology in a region of high hydroclimate variability. However, these short analysis periods are fairly well representative of the extended period of 1982–2006. Comparing each site's monthly mean precipitation climatology for both time periods yields a typical percent difference of 8% in the annual mean, a root-mean-square difference of 8 mm/month, and a temporal correlation (N = 12 months) of 0.88. Given that the mean precipitation annual cycles during these analysis periods are quite similar to the long-term climatology, it is likely that the mean soil moisture annual cycles during the analysis periods are also fairly representative of the long-term climatology.

[36] The importance of snowmelt for supplying a springtime surge of soil moisture for plant growth is assessed in EXP_SNOW (not shown), in which the snowpack is allowed to melt but resulting meltwater is not allowed to enter the soil. By comparing this sensitivity experiment with the control LPJ simulation, it is clear that snowmelt provides a critical boost of moisture to the entire soil column during March–June across sites in Utah and Colorado, which enhances July–September plant growth and amplifies the unimodal seasonal cycle of plant greenness.

3.4. Annual Cycle: Evapotranspiration

[37] In LPJ, total ET consists of plant transpiration, bare soil evaporation, and evaporation of canopy-intercepted precipitation (canopy intercepts falling precipitation and later evaporates the moisture) (Figures 4f and 5f). On averaged, 89% of simulated SWUS ET is due to transpiration, ranging from 76% in February to 92% in October. Simulated SWUS transpiration averages 23 cm annually and peaks in May and August. The simulated May transpiration peak over Utah and Colorado sites represents abundant transpiration from trees as they access soil moisture from earlier winter precipitation and spring snowmelt. *Hamlet et al.* [2007] likewise found that springtime snowmelt in the Colorado River Basin supports a late spring–early summer peak in soil moisture and ET. The simulated August transpiration peak, mainly in New Mexico, is attributed to grasses during their growing season, which tap into wet soils produced by monsoon rainfall. The simulated bimodal transpiration at Arizona–New Mexico sites includes peaks in March–May and August. Bare soil evaporation accounts for 22% of the total SWUS ET in February and is largest in July–August over southern Arizona–New Mexico.

[38] There is very little observational data for ET partitioning, with few, largely uncertain measurements. *Huxman et al.* [2005] summarized several empirical studies of ET partitioning at Chihuahuan, Sonoran, Mojave, and Great Basin sites and found a vast range in the partitioning, with transpiration accounting for 7%–85% of ET. Despite the uncertainty, we suspect that LPJ overemphasizes transpiration in its ET partitioning.

[39] The mean seasonal cycle of total ET is assessed from LPJ, site observations, MODIS diagnostic estimates, NARR, Willmott-Matsuura (WM) water budget analysis, and two hydrologic models, CPC and VIC (Figure 6). The annual mean LPJ-simulated ET at the 10 sites is significantly correlated ($p < 0.1$) with all these data sets, including $r = 0.74$ with MODIS. LPJ's results, which fall within the spread of ET data sets, are most similar to MODIS's ET measure, with a typical difference of ± 4.0 cm/yr among the sites. The annual mean ET, averaged among the 10 sites,

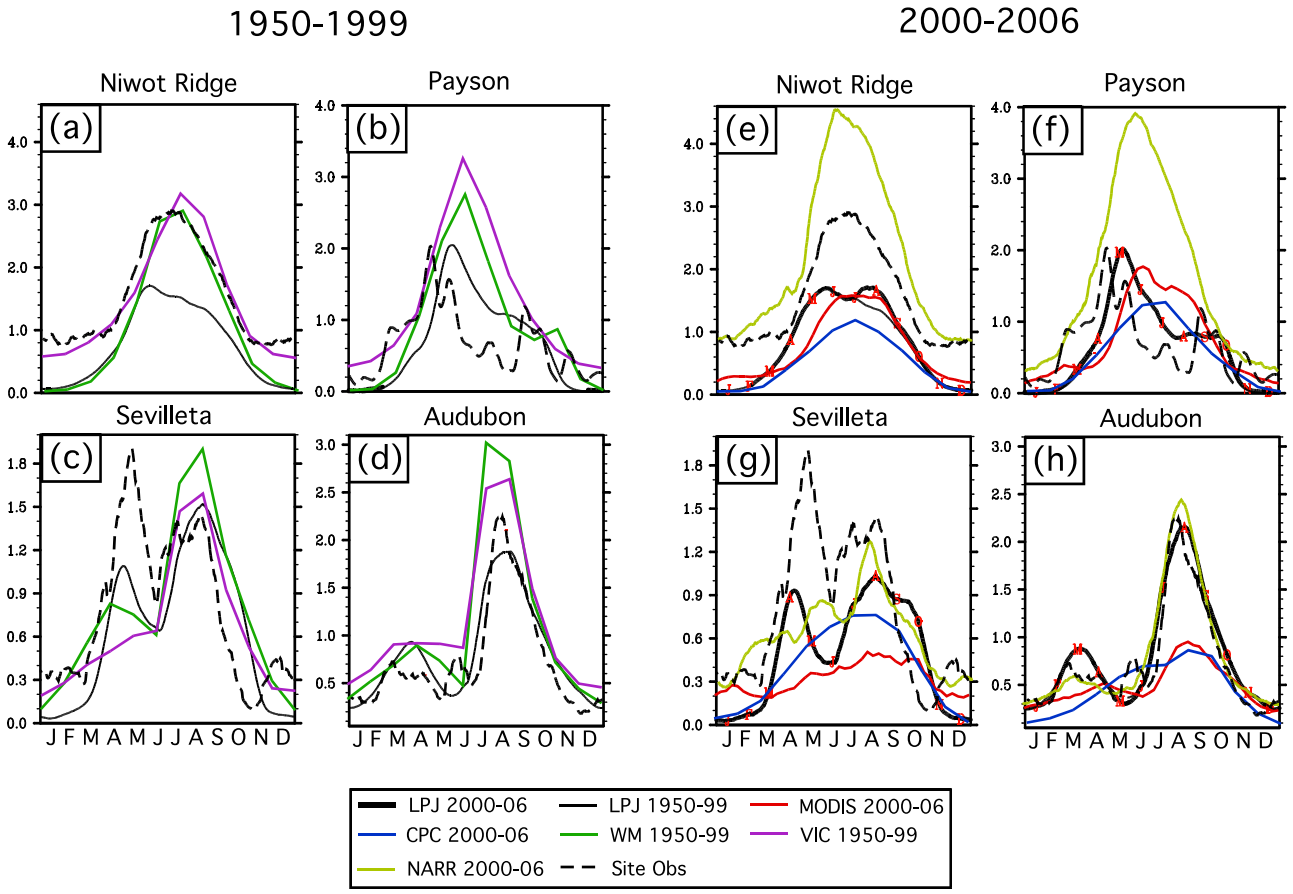

Figure 6. Mean seasonal cycle of evapotranspiration (mm/d) for (a–d) 1950–1999 and (e–h) 2000–2006 at Niwot Ridge, Payson, Sevilleta, and Audubon from LPJ (solid black), MODIS (red), CPC (blue), WM (green), VIC (purple), NARR (yellow), and site observations (dashed black; time period varies by site). Two periods are shown for LPJ to aid in comparing with other data sets, since certain data sets (e.g., WM) cover 1950–1999 and others (e.g., MODIS) cover 2000–2006.

ranges dramatically from 15.0 cm/yr for CPC to 46.4 cm/yr for NARR (see *Vivoni et al.* [2008] regarding NARR's wet soil bias in SWUS), while the LPJ mean (22.6 cm/yr) is close to MODIS estimates (20.8 cm/yr). Compared to LTER site measurements, *Mielnick et al.* [2005], and *Ivans et al.* [2006], LPJ underestimates ET at Niwot Ridge, Jornada Basin, and Sevilleta and accurately simulates it at Audubon and Payson; however, these local ET measurements may not be representative of large grid cells.

[40] Based on LPJ, MODIS, and the other evaporation data sets, ET is strongest at Baldy, due to wet soil and year-round transpiring evergreens, and weakest at Jornada Basin, due to dry soil and limited plants. Annual mean ET is larger among the forested sites (LPJ = 27.4 cm/yr, MODIS = 26.3 cm/yr) than among the grassland-shrubland sites (LPJ = 18.3 cm/yr, MODIS = 15.0 cm/yr). The correlation between GCFVC forest cover fraction and MODIS annual ET estimates for the 10 sites is 0.84 ($p < 0.01$). Based on MODIS estimates, ET is least over barren/sparse vegetation and greatest over evergreen forests. The LPJ-simulated ratio of annual ET to precipitation (ET/P) ranges from 0.62 to 0.82 among the 10 sites.

[41] At Niwot Ridge, all the data sets display a single, summertime ET peak (Figure 6). A springtime ET peak is simulated by LPJ over northern and western Utah, in response to moist soils from snowmelt and emerging vegetation; which agrees, in timing and magnitude, with observed ET measurements at Rush Valley (Figure 6). LPJ simulates a dual ET peak at the five Arizona–New Mexico sites, which is supported by NARR and WM for all five sites, by MODIS for the Arizona sites, and by site observations for Sevilleta and somewhat for Audubon and Jornada Basin (Figure 6). Although the New Mexico sites display mostly unimodal precipitation, simulated and observed dual peaks in soil moisture and ET are produced. VIC, WM, and LPJ results compare most favorably with site measurements.

3.5. Bimodal Seasonal Cycle of Vegetation

[42] Further evidence for, and understanding of, a bimodal seasonal cycle of vegetation greenness at Sevilleta and Jornada Basin are found using ground observations of species' phenology. The number of plant species within each phenological stage from the Sevilleta LTER Plant Phenology Transects data set is tallied for 1991–1993 (Figure 7). In all 3 years, the remotely sensed NDVI minimum, occurring sometime during June–July, coincides with ground observations of minima in the active phenology phases of

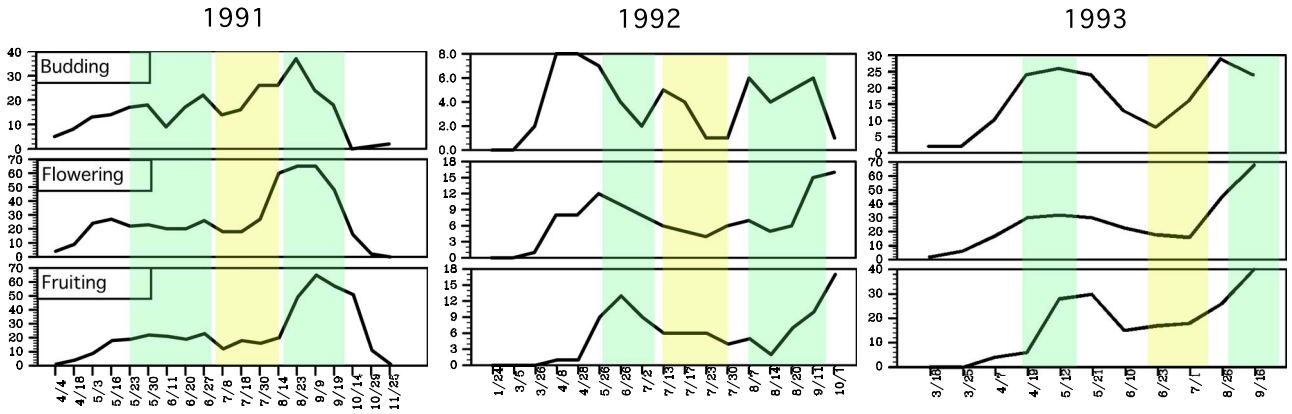

Figure 7. Number of plant species by date within the phenological stages of budding, flowering, and fruiting at Sevilleta, NM, during 1991–1993, based on the Sevilleta LTER Plant Phenology Transects data set. Data is analyzed for 145 species at four sites (Goat Draw/Cerro Montosa, Five Points/Deep Well, Rio Salado, and Red Tank/222) in 1991, for 56 species at the Five Points/Deep Well site in 1992, and 175 species at all four sites in 1993, based on sufficient data availability. The vertical yellow and green bars indicate the approximate time of the NDVI minimum and maxima for each year, respectively, using data from *Weiss et al.* [2004b].

budding, flowering, and fruiting, particularly for forbs, herbs, and graminoids.

[43] The LTER Plant Phenology Transect data set for Jornada Basin, for 1993–2004, reveals similar evidence for a bimodal seasonal cycle of vegetation phenology. Six key species are considered: *Dalea purpurea* (DAPU), *Bouteloua eriopoda* (BOER), *Panicum obtusum* (PAOB), *Hilaria mutica Benth.* (PLMU), *Scleropogon brevifolius* (SCBR), and *Larrea tridentate* (LATR). An initial budding peak occurs in April, particularly for the C3 shrub, LATR. This is followed by a flowering peak in May, mainly LATR and BOER. These coincide with the first NDVI remotely sensed peak in May. Next, a minimum in plant activity coincides with the June–July NDVI minimum. Late season peaks in budding (DAPU, BOER) during August–September, in flowering (BOER, PLMU, SCBR) during August–October, and fruiting (PAOB, BOER, SCBR) during September–November coincide with the August–October second NDVI peak. While the photosynthetic pathway of plants, and its relationship to temperature, might contribute to the bimodal seasonal cycle of vegetation activity, with C3 plants dominating earlier in the year than C4 plants, the active periods for C3 and C4 plant species often overlap throughout the year, making such a conclusion uncertain.

[44] The mechanism for bimodal NDVI is investigated through a pair of experiments, EXP_SOIL, applying a water scalar criterion of either 0.0 (grasses never wilt due to low soil moisture) or 0.2 (grasses are more sensitive to low soil moisture). The simulated NDVI dip during May–July at Sevilleta, Jornada Basin, Happy Jack, and Baldy amplifies when the criterion is set to 0.2 and disappears when set to 0.0, suggesting that plant sensitivity to soil moisture, represented by the water scalar factor, is the driving mechanism of the dual NDVI peak (Figure 8). This conclusion is reinforced by Figures 4d and 5d, which show that an observed minimum in soil moisture precedes the summertime collapse in NDVI at these locations, as existing species become phenologically inactive due to limited moisture availability. Among the control and two experiments, the simulated NDVI is actually lowest when the water scalar criterion is set to 0.0. When the grass is not permitted to wilt during periods of drought and high respiration cost, it is vulnerable to die-off, so the mean fractional cover of grass is lowest in this experiment. This suggests that the productivity of grasses is dependent on its ability to respond to drought.

[45] In order to test the hypothesis that the initial springtime NDVI surge produces substantial transpiration, dries the soil column, and triggers a drought response of wilting, experiment EXP_TRANSP is performed, in which plant transpiration during March–June is not permitted to exceed 0.3 mm/d. This criterion was selected since the selected site, Jornada Basin, which displays a bimodal NDVI seasonal cycle in the control simulation, experiences springtime transpiration in excess of 0.3 mm/d (Figure 5f). By preventing the springtime transpiration peak, the soil remains wetter and the drought response of wilting is avoided at Jornada Basin, Sevilleta, and Happy Jack, thereby eliminating the pattern of a bimodal NDVI seasonal cycle.

[46] The spatial distribution of the satellite-based dual NDVI peak is computed using the mean 0.5° × 0.5° NDVI seasonal cycle for 1982–2006 (Figure 9a). The observed dual peak covers 15% of the SWUS (N = 100 grid cells), stretching from northwest to southeast across Arizona and New Mexico. While much of Arizona exhibits a dual rainfall peak, the eastern portion into New Mexico is mainly dominated by a single monsoon peak in rainfall, yet it contains a dual NDVI peak. The model reproduces this region of dual NDVI peak stretching northwest to southeast across Arizona and New Mexico (Figure 9b), similarly consisting of 17% of the SWUS (N = 116).

[47] In experiment EXP_PREC (not shown), the seasonal cycles of monthly precipitation amount and frequency are replaced by annual mean values. The lack of a precipitation seasonal cycle does dampen the pattern of bimodal greening but the complete mechanism for this bimodal pattern is attributed to a seasonal interaction between precipitation and temperature, such that a region (e.g., Sevilleta and Jornada

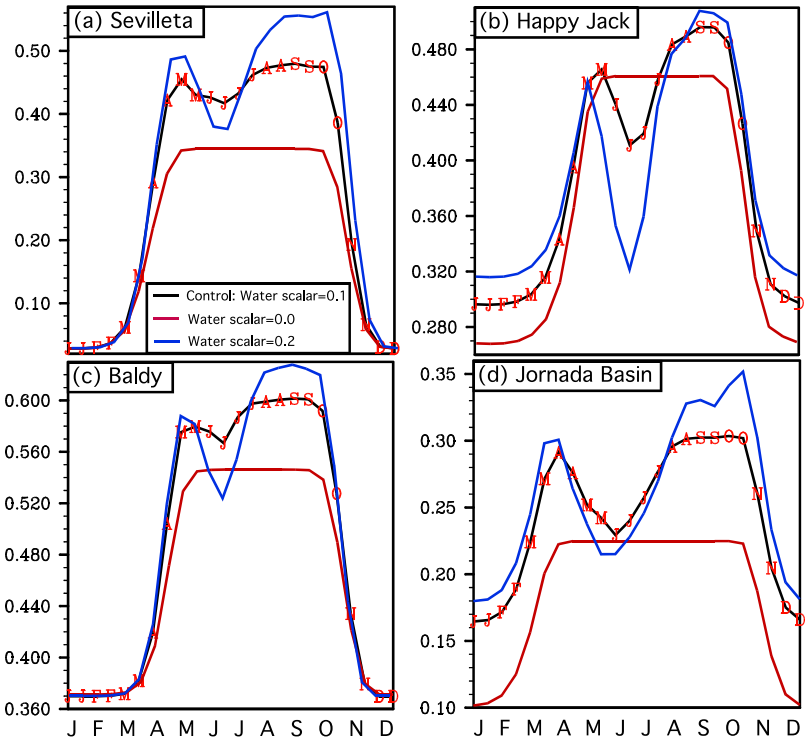

Figure 8. Mean seasonal cycle of simulated NDVI for (a) Sevilleta, (b) Happy Jack, (c) Baldy, and (d) Jornada Basin, averaged over 1901–2006, from the control run (black). By default, the control run uses a water scalar of 0.1, which is a weighted measure of total soil moisture fraction below which drought deciduous plants shed their leaves or wilt. Also shown for two experiments using water scalars of 0.0 (red, no wilting) and 0.2 (blue, more wilting).

Basin) dominated by single peak in precipitation can display a dual peak in soil moisture and thus NDVI. For such locations, the initial peak in soil moisture is attributed to an accumulation of soil moisture from weak wintertime precipitation events and minimal transpiration, while the latter peak is associated with summer monsoon precipitation.

[48] The impact of warming associated with climate change on the seasonal cycle of SWUS vegetation is assessed with EXP_TEMP, in which the 1901–2006 simulation is repeated with a uniform temperature increase of 5°C, reflecting the predicted 21st century SWUS warming in the A2 scenario of IPCC AR4. This warming results in a 29% increase in the area with simulated bimodal NDVI, now covering 150 grid cells (Figure 9c). Higher temperatures and greater evaporation dry the soil in summer, thereby enhancing summertime plant wilting from drought and shifting both soil moisture and vegetation from a unimodal cycle to a bimodal cycle.

4. Discussion

[49] This study examines the seasonal cycles, and associated climatic controls, of vegetation productivity, soil moisture, and ET across the SWUS, focusing on 10 select sites representative of diverse SWUS ecosystems. When a global dynamic vegetation-hydrology model (LPJ) is applied across a topographically and ecologically complex region, it is necessary to carefully adapt the model's climatic thresholds for that region and to use the most reliable climatic forcing data. Upon doing so, LPJ produces a simulation that agrees fairly well with observations in terms of the spatial distribution, time series, and seasonal cycle of SWUS vegetation. Due to the coarseness of the gridded climate data, LPJ underestimates the high spatial variability in both climate and vegetation across the SWUS, including an underestimation of simulated evergreen tree cover across the higher elevations of Arizona and New Mexico.

[50] The seasonal progression of peak NDVI occurs spatially in a clockwise fashion across the SWUS, beginning in spring across the Sonoran Desert in response to winter rains, then across Utah-Colorado due to snowmelt/summer rains, and finally in New Mexico–eastern Arizona associated with late summer monsoon rains. Vegetation in the SWUS is largely water limited, but temperature also significantly regulates plant growth at high elevations and regions with large seasonal/diurnal temperature cycles. Temperature, when expressed in growing degree days, regulates carbon assimilation, while temperature extremes limit plant distribution.

[51] The dramatic SWUS droughts during the 1930s, 1950s, and 1990s to 2000s produce substantial vegetation mortality based on site observations and LPJ simulations. LPJ produces excessive loss of leaf cover during drought years (auxiliary material). By clumping diverse plant species into single PFTs with uniform characteristics, LPJ fails to capture the drought resistance and deep roots of some

plants; LPJ also does not include a succulent PFT, which is capable of storing and drawing on water reserves during dry periods. LPJ neglects deep groundwater resources beyond its 1.5 m soil column, which may be critical for drought survival. The absence of anthropogenic fire suppression likely contributes to exaggerated drought responses. Severe droughts can dramatically alter the landscape for subsequent decades. The simulated land carbon storage takes more than a decade to recover from such events. Higher temperatures and increased evaporation associated with rising concentrations of greenhouse gases are projected to increase the frequency and severity of drought episodes.

[52] The impact of droughts on SWUS vegetation requires further studies, ideally using methods of conditional statistics that can identify thresholds for mortality as a function of drought duration. Likely, plant species in such semiarid environments have adapted to high interannual variability in precipitation and frequent droughts but are vulnerable to extended, multiyear drought events. Wavelet analysis of remotely sensed NDVI reveals a peak in power around 4 years in the northern Chihuahuan sites of Sevilleta and Jornada Basin. This is further explored in LPJ, with a wavelet analysis of Sevilleta's simulated annual vegetation cover fraction revealing power at 4–8 years, dominated by the prolonged droughts of the 1920s and 1990s to 2000s. Cross-spectrum analysis of annual precipitation and simulated vegetation cover fraction identifies significant coherence at 5 years for Sevilleta and both 2 years and 8–12 years for Jornada Basin, as multiyear droughts trigger substantial vegetation die-off. Analysis of remotely sensed NDVI data indicates that Sevilleta and Jornada Basin are the most sensitive sites to multiyear droughts, with reductions in annual NDVI that are twice as large in multiyear than single year droughts. These initial drought mortality results warrant further investigation.

[53] The seasonal cycles of climate, vegetation greenness, soil moisture, and evaporation are analyzed at five high-elevation, forested and five grassland-shrubland sites using observations and LPJ simulations. For the high-altitude sites, the timing of spring-summer warming and snowmelt, which resupplies soil water, is critical for vegetation greening. At warmer, semiarid locations, vegetation relies either on weaker winter-spring precipitation events associated with frontal activity, or on intense convective rainfall events during the summer monsoon. There is substantial spread among estimates of the seasonal cycle of ET among remote sensing, water budget, and hydrology model data sets, so caution should be applied when using such data sets since little is known about actual observed fluxes. LPJ's prognostic ET falls within the envelope of uncertainty of the various ET data sets and agrees most closely with MODIS' diagnostic ET estimates. The forested sites consistently exhibit greater ET than grassland-shrubland sites. It appears that LPJ underestimates soil evaporation in semiarid regions despite the soil hydrology improvements by *Gerten et al.*

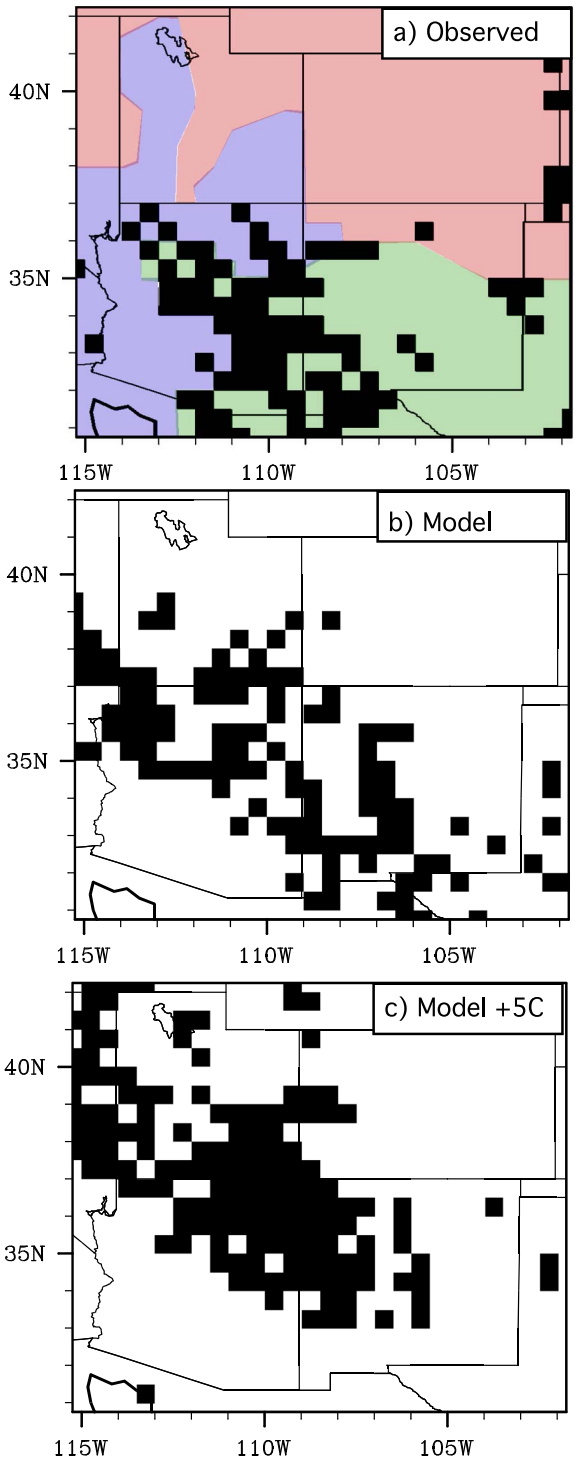

Figure 9. Area with a bimodal NDVI seasonal cycle based on (a) GIMMS satellite data, (b) the model control run, and (c) the model experiment with 5°C warming, all with a 0.5° × 0.5° resolution. A grid cell is identified as bimodal, with black shading, if there are two peaks, with a relative minimum in between at least 0.02 lower than the peaks, based on the mean 1982–2006 seasonal cycle of NDVI. As a test of robustness, if a criterion of 0.04 is applied, both the observations and model show an area of bimodal NDVI seasonal cycle across central Arizona through western New Mexico, although less extensive in area with the observations. In Figure 9a, the three colors indicate the season of maximum observed NDVI, with blue for winter-spring (DJF-MAM), red for summer (JJA), and green for autumn (SON).

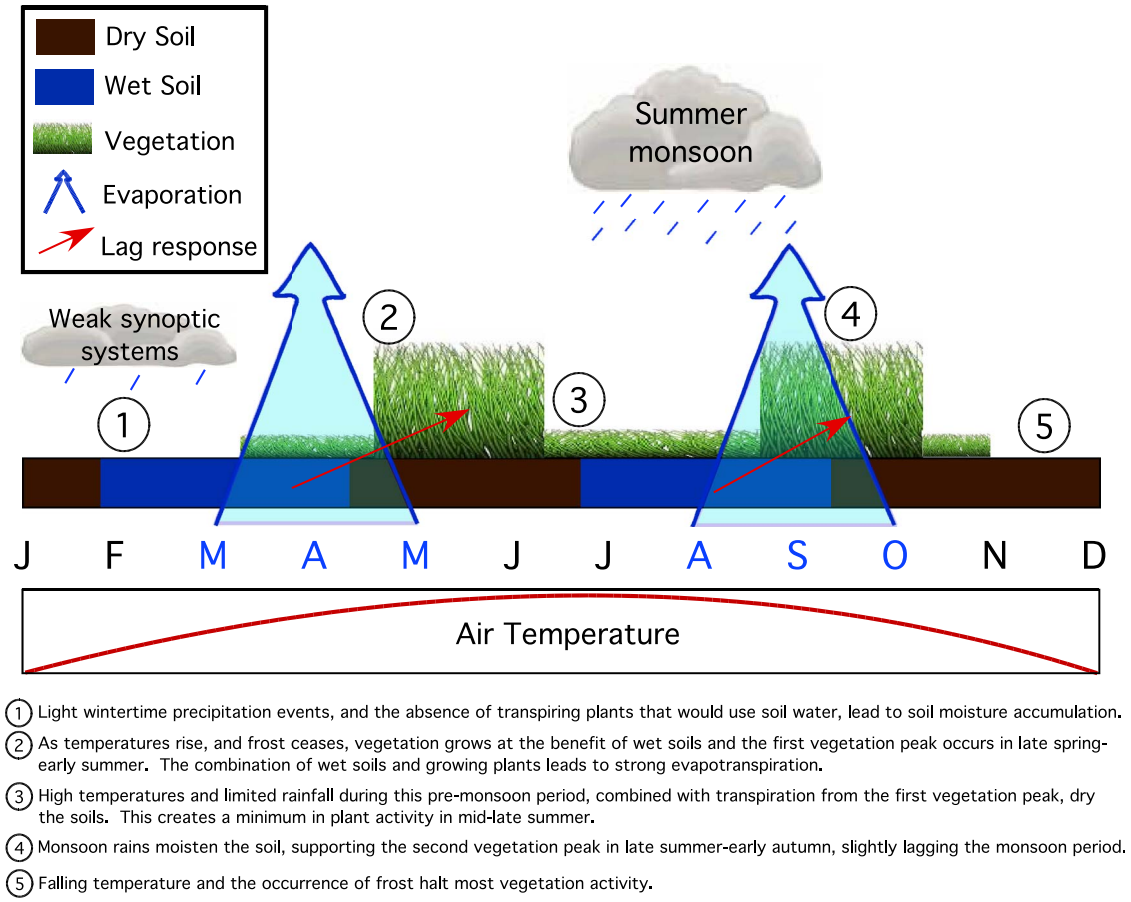

Figure 10. Schematic explaining the bimodal NDVI seasonal cycle in the North American monsoon region.

[2004]. To better constrain the model, more extensive observations are needed of total ET and its partitioning, along with soil moisture, potentially through advances in remote sensing techniques.

[54] Satellite observations and LPJ simulations exhibit a bimodal NDVI seasonal cycle at Sevilleta, Jornada Basin, Baldy, and Happy Jack. The observed and simulated region of bimodal NDVI stretches from northwest to southeast across Arizona and New Mexico. Observations and LPJ simulations suggest the following mechanism for this bimodal seasonal cycle of vegetation phenology (Figure 10). During the cold season, when most plants are dormant or dead, soil moisture accumulates in response to weak precipitation events. At sites with substantial snowfall, springtime snowmelt also recharges the soil moisture. Once the cold season and its associated dormancy ends, an initial vegetation surge occurs, benefiting from stored deep soil moisture. This typically consists of annuals and C3 cool-season shrubs, which rely on deep moisture. Limited precipitation and continually rising temperatures deplete soil moisture in early mid summer, while plant transpiration from the initial green-up is an ongoing moisture sink, leading to early mid summer plant dormancy and NDVI minimum. In LPJ, the drought-related water scalar term, representing available soil moisture, triggers the loss of leaves or plant dormancy, thus creating an NDVI minimum. Both transpiration from the initial springtime green-up, which dries the soil column, and the drought response of wilting/dormancy to the dry soil in early mid summer, are required to produce a simulated bimodal NDVI seasonal cycle. The seasonal pattern of two NDVI peaks is hydrologically driven in LPJ. Field measurements at Sevilleta and Jornada Basin reveal that the early mid summer NDVI minimum corresponds to minima in plant budding, flowering, and fruiting. Finally, the monsoon rains arrive around July (Figures 4b and 5b), recharging soil moisture and boosting plant activity, manifested as a late summer–early autumn green-up that produces the second, greater NDVI peak. Eventually plant activity reduces with falling autumn-winter temperatures. The observed dual peak in soil moisture and NDVI, with the minimum in NDVI just prior to the monsoon rains, gives credibility to this proposed mechanism. Future warming may expand the region experiencing a bimodal NDVI seasonal cycle by intensifying summertime, premonsoon soil drying.

[55] The mechanism presented here for the bimodal seasonal cycle of vegetation green-up in some semiarid regions of the SWUS is consistent with the proposed mechanism of *Muldavin et al.* [2008] for Sevilleta, based on 6 years of ANPP records. Both our study and that of *Muldavin et al.*

[2008] argue that the pulse-reserve paradigm is applicable in late summer as heavy, transient monsoon rainstorms provide pulses of upper soil moisture, supporting the greening of C4 grasses, forbs, shallow-rooted subshrubs, and Crassulacean acid metabolism (CAM) succulents. Large summertime ET fluxes also restrict soil moisture accumulation [*Bhark and Small*, 2003; *Kurc and Small*, 2004]. However, both studies find the pulse-reserve paradigm is insufficient for explaining the late springtime green-up. Deep-rooted C3 shrubs, C3 grasses, forbs, and subshrubs are responding at that time to a break in cold dormancy and benefit from an accumulation of deep soil moisture from low-intensity (ENSO- or PDO-related) precipitation events that occurred throughout winter [*Molles and Dahm*, 1990; *Gutzler et al.*, 2002], rather than recent pulses of rainfall. In agreement with *Muldavin et al.* [2008], this study finds that the springtime greening is more analogous to the response of temperate ecosystems to the arrival of spring rather than the traditional pulse precipitation mechanism.

[56] **Acknowledgments.** The authors appreciate the helpful discussion and contributions from Debra Peters, Qiaozhen Mu, and Dieter Gerten and the detailed suggestions from two reviewers and two editors. The study was funded by DOE NICCR and NOAA CPPA. This is Nelson Institute Center for Climatic Research publication 996.

References

Andrade, E. R., Jr., and W. D. Sellers (1988), El Niño and its effect on precipitation in Arizona and western New Mexico, *J. Clim.*, *8*, 403–410, doi:10.1002/joc.3370080407.

Arora, V. K., and G. J. Boer (2006), Simulating competition and coexistence between plant functional types in a dynamic vegetation model, *Earth Interact.*, *10*(10), 1–30.

Asrar, G., M. Fuchs, E. T. Kanemasu, and J. L. Hatfield (1984), Estimating absorbed photosynthetically active radiation and leaf area index from spectral reflectance in wheat, *Agron. J.*, *76*, 300–306, doi:10.2134/agronj1984.00021962007600020029x.

Baker, F. S. (1925), *Aspen in the Central Rocky Mountain Region, U.S. Dep. Agric. Bull.*, vol. 1291, 47 pp., U.S. Dep. of Agric., Washington, D. C.

Baret, F., and O. Olioso (1989), Estimation à partir de measures de réflectance spectrale du rayonnement photosynthétiquement actif absorbé par une culture de blé, *Agronomie*, *9*, 885–895, doi:10.1051/agro:19890906.

Betancourt, J. L., E. A. Pierson, K. A. Rylander, J. A. Fairchild-Parks, and J. S. Dean (1993), Influence of history and climate on New Mexico piñon-juniper woodlands, in *Managing Piñon-Juniper Ecosystems for Sustainability and Social Needs, Gen. Tech. Rep. RM 236*, edited by E. F. Aldon and D. W. Shaw, pp. 42–62, U.S. Dep. of Agric., Washington, D. C.

Bhark, E. W., and E. E. Small (2003), The relationship between plant canopies and the spatial patterns of infiltration in shrubland and grassland of the Chihuahuan Desert, New Mexico, *Ecosystems*, *6*, 185–196, doi:10.1007/s10021-002-0210-9.

Bosilovich, M. G., and S. D. Schubert (2002), Water vapor tracers as diagnostics of the regional hydrologic cycle, *J. Hydrometeorol.*, *3*, 149–165, doi:10.1175/1525-7541(2002)003<0149:WVTADO>2.0.CO;2.

Breshears, D. D., et al. (2005), Regional vegetation die-off in response to global-change-type drought, *Proc. Natl. Acad. Sci. U. S. A.*, *102*, 15,144–15,148, doi:10.1073/pnas.0505734102.

Brown, A. B. (1935), Cambial activity, root habit and sucker shoot development in two species of poplar, *New Phytol.*, *34*, 163–179, doi:10.1111/j.1469-8137.1935.tb06839.x.

Carleton, A. M., D. A. Carpenter, and P. J. Weser (1990), Mechanisms of interannual variability of Southwest United States summer precipitation maximum, *J. Clim.*, *3*, 999–1015, doi:10.1175/1520-0442(1990)003<0999:MOIVOT>2.0.CO;2.

Carter, R. (2003), Climate, forest management stoke western wildfires: CLIMAS southwest climate outlook, 4 pp., Univ. of Ariz, Tucson.

Chen, F., Z. Janji, and K. Mitchell (1997), Impact of atmospheric surface-layer parameterizations in the new land-surface scheme of the NCEP mesoscale Eta model, *Boundary Layer Meteorol.*, *85*, 391–421, doi:10.1023/A:1000531001463.

Christensen, J. H., et al. (2007), Regional climate projections, in *Climate Change 2007: The Physical Science Basis: Contribution of Working Group 1 to the Fourth Assessment Report of the Intergovernmental Panel on Climate Change*, edited by S. Solomon et al., pp. 847–940, Cambridge Univ. Press, New York.

Cleugh, H. A., R. Leuning, Q. Mu, and S. W. Running (2007), Regional evaporation estimates from flux tower and MODIS satellite data, *Remote Sens. Environ.*, *106*, 285–304, doi:10.1016/j.rse.2006.07.007.

Cornelius, J. M., P. R. Kemp, J. A. Ludwig, and G. L. Cunningham (1991), The distribution of vascular plant species and guilds in space and time along a desert gradient, *J. Vegetation Sci.*, *2*, 59–72.

Daughtry, C. S. T. (1988), Estimating absorbed radiation and phytomass from multispectral reflectance of corn and soybeans, in *Proceedings of 1988 International Geoscience and Remote Sensing Symposium*, pp. 821–824, Eur. Space Agency, Neuilly, France.

Day, M. W. (1944), The root system of Aspen, *Am. Midl. Nat.*, *32*, 502–509, doi:10.2307/2421314.

DeFries, R. S., J. R. G. Townshend, and M. C. Hansen (1999), Continuous fields of vegetation characteristics at the global scale at 1-km resolution, *J. Geophys. Res.*, *104*, 16,911–16,925, doi:10.1029/1999JD900057.

DeFries, R. S., M. C. Hansen, J. R. G. Townshend, A. C. Janetos, and T. R. Loveland (2000a), A new global 1-km dataset of percentage tree cover derived from remote sensing, *Global Change Biol.*, *6*, 247–254, doi:10.1046/j.1365-2486.2000.00296.x.

DeFries, R. S., M. C. Hansen, and J. R. G. Townshend (2000b), Global continuous fields of vegetation characteristics: A linear mixture model applied to multi-year 8 km AVHRR data, *Int. J. Remote Sens.*, *21*, 1389–1414, doi:10.1080/014311600210236.

Fensholt, R., I. Sandholt, and M. S. Rasmussen (2004), Evaluation of MODIS LAI, fAPAR and the relation between fAPAR and NDVI in a semi-arid environment using in situ measurements, *Remote Sens. Environ.*, *91*, 490–507, doi:10.1016/j.rse.2004.04.009.

Gerten, D., S. Schaphoff, U. Haberlandt, W. Lucht, and S. Sitch (2004), Terrestrial vegetation and water balance hydrological evaluation of a dynamic global vegetation model, *J. Hydrol.*, *286*, 249–270, doi:10.1016/j.jhydrol.2003.09.029.

Gosz, J. (1994), Plant Phenology Transects, http://sev.lternet.edu/project_details.php?id=SEV048, Sevilleta Long Term Ecol. Res. Site Database, Albuquerque, N. M.

Guirguis, K. J., and R. Avissar (2008), A precipitation climatology and dataset intercomparison for the western United States, *J. Hydrometeorol.*, *9*, 825–841, doi:10.1175/2008JHM832.1.

Gutzler, D. S. (2000), Covariability of spring snowpack and summer rainfall across the Southwest United States, *J. Clim.*, *13*, 4018–4027, doi:10.1175/1520-0442(2000)013<4018:COSSAS>2.0.CO;2.

Gutzler, D. S., and J. W. Preston (1997), Evidence for a relationship between spring snow cover in North America and summer rainfall in New Mexico, *Geophys. Res. Lett.*, *24*, 2207–2210, doi:10.1029/97GL02099.

Gutzler, D. S., D. M. Kann, and C. Thornbrugh (2002), Modulation of ENSO-based long-lead outlooks of southwestern U.S. winter precipitation by the Pacific decadal oscillation, *Weather Forecasting*, *17*, 1163–1172, doi:10.1175/1520-0434(2002)017<1163:MOEBLL>2.0.CO;2.

Hadley, N. F., and S. R. Szarek (1981), Productivity of desert ecosystems, *BioScience*, *31*, 747–753, doi:10.2307/1308782.

Hall, F. G., K. F. Huemmrich, S. J. Goetz, P. J. Sellers, and J. E. Nickeson (1992), Satellite remote sensing of surface energy balance: Success, failures, and unresolved issues in FIFE, *J. Geophys. Res.*, *97*, 19,061–19,089.

Hamlet, A. F., P. W. Mote, M. P. Clark, and D. P. Lettenmaier (2007), Twentieth-century trends in runoff, evapotranspiration, and soil moisture in the western United States, *J. Clim.*, *20*, 1468–1486, doi:10.1175/JCLI4051.1.

Hawkins, T. W., and A. W. Ellis (2007), A case study of the energy budget of a snowpack in the arid, subtropical climate of the southwestern United States, *J. Ariz. Nev. Acad. Sci.*, *39*, 1–13, doi:10.2181/1533-6085(2007)39[1:ACSOTE]2.0.CO;2.

Herbel, C. H., F. N. Ares, and R. A. Wright (1972), Drought effects on a semidesert grassland range, *Ecology*, *53*, 1084–1093, doi:10.2307/1935420.

Higgins, R. W., and W. Shi (2001), Intercomparison of the principal modes of interannual and intraseasonal variability of the North American monsoon system, *J. Clim.*, *14*, 403–417, doi:10.1175/1520-0442(2001)014<0403:IOTPMO>2.0.CO;2.

Higgins, R. W., K. C. Mo, and Y. Yao (1998), Interannual variability of the U.S. summer precipitation regime with emphasis on the southwestern monsoon, *J. Clim.*, *11*, 2582–2606, doi:10.1175/1520-0442(1998)011<2582:IVOTUS>2.0.CO;2.

Huang, J., H. van den Dool, and K. P. Georgakakos (1996), Analysis of model-calculated soil moisture over the United States (1931–93) and application to long-range temperature forecasts, *J. Clim.*, *9*, 1350–1362, doi:10.1175/1520-0442(1996)009<1350:AOMCSM>2.0.CO;2.

Huang, Z., and C. A. Lai (1998), Multidecadal variability on the southwestern United States monsoon precipitation in the past century, in *Ninth Conference on Interaction of the Sea and Atmosphere*, edited by American Meteorological Society, pp. 159–166, Phoenix, Ariz.

Huenneke, L., and D. Peters (1992), Plant Phenology Transects at NPP Sites, http://jornada-www.nmsu.edu/studies/lter/datasets/plants/nppphen/phentran.dsd, Jornada Basin Long Term Ecol. Res. Site Database, Albuquerque, N. M.

Huxman, T. E., et al. (2005), Ecohydrological implications of woody plant encroachment, *Ecology*, *86*, 308–319, doi:10.1890/03-0583.

Isard, S. A. (1986), Factors influencing soil moisture and plant community distribution on Niwot Ridge, Front Range, Colorado, *U.S.A., Arct. Alp. Res.*, *18*, 83–96, doi:10.2307/1551216.

Ivans, S., L. Hipps, A. J. Leffler, and C. Y. Ivans (2006), Response of water vapor and CO_2 fluxes in semiarid lands to seasonal and intermittent precipitation pulses, *J. Hydrometeorol.*, *7*, 995–1010, doi:10.1175/JHM545.1.

Justice, C. O., J. R. G. Townshend, B. N. Holben, and C. J. Tucker (1985), Analysis of the phenology of global vegetation using meteorological satellite data, *Int. J. Remote Sens.*, *6*, 1271–1318, doi:10.1080/01431168508948281.

Kemp, P. R., (1983), Phenological patterns of Chihuahuan Desert plants in relation to the timing of water availability, *J. Ecol.*, *71*, 427–436, doi:10.2307/2259725.

Kremer, R. G., and S. W. Running (1993), Community type differentiation using NOAA/AVHRR data within a sagebrush-steppe ecosystem, *Remote Sens. Environ.*, *46*, 311–318, doi:10.1016/0034-4257(93)90051-X.

Kurc, S. A., and E. E. Small (2004), Dynamics of evapotranspiration in semiarid grassland and shrubland ecosystems during the summer monsoon season, central New Mexico, *Water Resour. Res.*, *40*, W09305, doi:10.1029/2004WR003068.

Kurc, S. A., and E. E. Small (2007), Soil moisture variations and ecosystem-scale fluxes of water and carbon in semiarid grassland and shrubland, *Water Resour. Res.*, *43*, W06416, doi:10.1029/2006WR005011.

Laliberte, A. S., A. Rango, K. M. Havstad, J. F. Paris, R. F. Beck, R. McNeely, and A. L. Gonzalez (2004), Object-oriented image analysis for mapping shrub encroachment from 1937 to 2003 in southern New Mexico, *Remote Sens. Environ.*, *93*, 198–210, doi:10.1016/j.rse.2004.07.011.

Lange, O. L., L. Kappen, and E. D. Schulze (1976), *Water and Plant Life*, 536 pp., Springer, New York.

Lizárraga-Celaya, C., C. J. Watts, J. C. Rodriguez, J. Garatuza-Payán, R. L. Scott, and J. Sáiz-Hernández (2010), Spatio-temporal variations in surface characteristics over the North American monsoon region, *J. Arid Environ.*, *74*, 540–548, doi:10.1016/j.jaridenv.2009.09.027.

Loveland, T. R., and A. S. Belward (1997), The IGBP-DIS global 1 km land cover data set, Discover: First results, *Int. J. Remote Sens.*, *18*, 3289–3295.

Loveland, T. R., B. C. Reed, J. F. Brown, D. O. Ohlen, J. Zhu, L. Yang, and J. W. Merchant (2001), Development of a global land cover characteristics database and IGBP DISCover from 1-km AVHRR data, *Int. J. Remote Sens.*, *21*, 1303–1330.

Lucht, W., et al. (2002), Climatic control of the high-latitude vegetation greening trend and Pinatubo effect, *Science*, *296*, 1687–1689, doi:10.1126/science.1071828.

Maurer, E. P., A. W. Wood, J. C. Adam, D. P. Lettenmaier, and B. Nijssen (2002), A long-term hydrologically based data set of land surface fluxes and states for the conterminous United States, *J. Clim.*, *15*, 3237–3251, doi:10.1175/1520-0442(2002)015<3237:ALTHBD>2.0.CO;2.

McDonald, J. E., (1956), Variability of precipitation in an arid region: A survey of characteristics for Arizona, *Tech. Rep. Meteorol. Climatol. Arid Reg. 1*, Inst. of Atmos. Phys., Univ. of Ariz., Tucson.

Mesinger, F., et al. (2006), North American regional reanalysis, *Bull. Am. Meteorol. Soc.*, *87*, 343–360, doi:10.1175/BAMS-87-3-343.

Mielnick, P., W. A. Dugas, K. Mitchell, and K. Havstad (2005), Long-term measurements of CO_2 flux and evapotranspiration in a Chihuahuan desert grassland, *J. Arid Environ.*, *60*, 423–436, doi:10.1016/j.jaridenv.2004.06.001.

Mitchell, T. D., and P. D. Jones (2005), An improved method of constructing a database of monthly climate observations and associated high-resolution grids, *Int. J. Climatol.*, *25*, 693–712, doi:10.1002/joc.1181.

Molles, M. C., Jr., and C. N. Dahm (1990), A perspective on El Niño and La Nina: Global implications for stream ecology, *J. N. Am. Benthol. Soc.*, *9*, 68–76, doi:10.2307/1467935.

Monteith, J. L. (1964), Evaporation and environment: The state and movement of water in living organisms, *Symp. Soc. Exp. Biol.*, *19*, 205–234.

Mu, Q., F. A. Heinsch, M. Zhao, and S. W. Running (2007a), Development of a global evapotranspiration algorithm based on MODIS and global meteorological data, *Remote Sens. Environ.*, *111*, 519–536, doi:10.1016/j.rse.2007.04.015.

Mu, Q., M. Zhao, F. A. Heinsch, M. Liu, H. Tian, and S. W. Running (2007b), Evaluating water stress controls on primary production in biogeochemical and remote sensing based models, *J. Geophys. Res.*, *112*, G01012, doi:10.1029/2006JG000179.

Muldavin, E. H., D. L. Moore, S. L. Collins, K. R. Wetherill, and D. C. Lightfoot (2008), Aboveground net primary production dynamics in a northern Chihuahuan Desert ecosystem, *Oecologia*, *155*, 123–132, doi:10.1007/s00442-007-0880-2.

Myneni, R. B., and D. L. Williams (1994), On the relationship between FAPAR and NDVI, *Remote Sens. Environ.*, *49*, 200–211, doi:10.1016/0034-4257(94)90016-7.

Myneni, R. B., F. G. Hall, P. J. Sellers, and A. L. Marshak (1995), The interpretation of spectral vegetation indexes, *IEEE Trans. Geosci. Remote Sens.*, *33*, 481–486, doi:10.1109/36.377948.

Myneni, R. B., R. Ramakrishna, R. Nemani, and S. W. Running (1997), Estimation of global leaf area index and absorbed par using radiative transfer models, *IEEE Trans. Geosci. Remote Sens.*, *35*, 1380–1393, doi:10.1109/36.649788.

Noy-Meir, I. (1973), Desert ecosystems: Environment and producers, *Annu. Rev. Ecol. Syst.*, *4*, 25–51, doi:10.1146/annurev.es.04.110173.000325.

O'Brien, R. A. (2002), Arizona's forest resources, 1999, *Resour. Bull. RMRS-RB-2*, U.S. Dep. of Agric. For. Serv., Ogden, Utah.

Ogle, K., T. G. Whitham, and N. S. Cobb (2000), Tree-ring variation in pinyon predicts likelihood of death following severe drought, *Ecology*, *81*, 3237–3243, doi:10.1890/0012-9658(2000)081[3237:TRVIPP]2.0.CO;2.

Paruelo, J. M., and W. K. Lauenroth (1996), Relative abundance of plant functional types in grasslands and shrublands of North America, *Ecol. Appl.*, *6*, 1212–1224, doi:10.2307/2269602.

Pennington, D. D., and S. L. Collins (2007), Response of an aridland ecosystem to interannual climate variability and prolonged drought, *Landscape Ecol.*, *22*, 897–910, doi:10.1007/s10980-006-9071-5.

Peters, A. J., and M. D. Eve (1995), Satellite monitoring of desert plant community response to moisture availability, *Environ. Monit. Assess.*, *37*, 273–287, doi:10.1007/BF00546895.

Pinzon, J., et al. (2004), Satellite time series correction of orbital drift artifacts using empirical mode decomposition, in *Hilbert-Huang Transform: Introduction and Applications*, part II, *Applications*, chap. 10, edited by N. Huang, pp. 167–186, World Sci., Hackensack, N. J.

Prince, S. D., S. J. Goetz, and S. N. Goward (1995), Monitoring primary productivity from Earth observing satellites, *Water Air Soil Pollut.*, *82*, 509–522, doi:10.1007/BF01182860.

Ramankutty, N., and J. A. Foley (1999), Estimating historical changes in global land cover: Croplands from 1700 to 1992, *Global Biogeochem. Cycles*, *13*(4), 997–1027, doi:10.1029/1999GB900046.

Reed, B. C., and K. Sayler (1998), A method for deriving phenological metrics from satellite data, Colorado 1991–1995, in *Proceedings of the Northern Great Plains Regional Workshop on Climate Change and Climate Variability*, edited by G. A. Seielstad et al., pp. 47–55, Univ. of N. D. Press, Grand Forks.

Reynolds, J. F., P. R. Kemp, and J. D. Tenhunen (2000), Effects of long-term rainfall variability on evapotranspiration and soil water distribution in the Chihuahuan Desert: A modeling analysis, *Plant Ecol.*, *150*, 145–159.

Ruimy, A., B. Saugier, and G. Dedieu (1994), Methodology for the estimation of terrestrial net primary production from remotely sensed data, *J. Geophys. Res.*, *99*, 5263–5283, doi:10.1029/93JD03221.

Schulman, E. (1956), *Dendroclimatic Change in Semiarid America*, 142 pp., Univ. of Ariz. Press, Tucson.

Scott, R. L., T. E. Huxman, W. L. Cable, and W. E. Emmerich (2006), Partitioning of evapotranspiration and its relation to carbon dioxide exchange in a Chihuahuan Desert shrubland, *Hydrol. Processes*, *20*, 3227–3243, doi:10.1002/hyp.6329.

Seager, R., Y. Kushnir, C. Herweijer, N. Naik, and J. Velez (2005), Modeling of tropical forcing of persistent droughts and pluvials over western North America: 1856–2000, *J. Clim.*, *18*, 4065–4088, doi:10.1175/JCLI3522.1.

Seager, R., et al. (2007), Model projections of an imminent transition to a more arid climate in southwestern North America, *Science*, *316*, 1181–1184, doi:10.1126/science.1139601.

Sellers, P. J. (1985), Canopy reflectance, photosynthesis, and transpiration, *Int. J. Remote Sens.*, *6*, 1335–1372, doi:10.1080/01431168508948283.

Shaw, J. D., B. E. Steed, and L. T. DeBlander (2005), Forest inventory and analysis (FIA) annual inventory answers the question: What is happening to pinyon-juniper woodlands?, *J. For.*, *103*, 280–285.

Shen, W., J. Wu, P. R. Kemp, J. F. Reynolds, and N. B. Grimm (2005), Simulating the dynamics of primary productivity of a Sonoran ecosystem: Model parameterization and validation, *Ecol. Modell.*, *189*, 1–24, doi:10.1016/j.ecolmodel.2005.04.010.

Shreve, F. (1942), The desert vegetation of North America, *Bot. Rev.*, *8*, 195–246, doi:10.1007/BF02882228.

Sitch, S., et al. (2000), LPJ-A coupled model of vegetation dynamics and the terrestrial carbon cycle, in The role of vegetation dynamics in the control of atmospheric CO_2 content, Ph.D. thesis, Lund Univ., Lund, Sweden.

Sitch, S., et al. (2003), Evaluation of ecosystem dynamics, plant geography and terrestrial carbon cycling in the LPJ dynamic global vegetation model, *Global Change Biol.*, *9*, 161–185, doi:10.1046/j.1365-2486.2003.00569.x.

Small, E. E. (2001), The influence of soil moisture anomalies on variability of the North American monsoon system, *Geophys. Res. Lett.*, *28*, 139–142, doi:10.1029/2000GL011652.

Spanner, M. A., L. L. Pierce, S. W. Running, and D. L. Peterson (1990), The seasonality of AVHRR data of temperate coniferous forests: Relationships with leaf area index, *Remote Sens. Environ.*, *33*, 97–112, doi:10.1016/0034-4257(90)90036-L.

Still, C. J., J. A. Berry, G. J. Collatz, and R. S. DeFries (2003), Global distribution of C_3 and C_4 vegetation: Carbon cycle implications, *Global Biogeochem. Cycles*, *17*(1), 1006, doi:10.1029/2001GB001807.

Swetnam, T. W., and J. L. Betancourt (1998), Mesoscale disturbance and ecological response to decadal climate variability in the American Southwest, *J. Clim.*, *11*, 3128–3147, doi:10.1175/1520-0442(1998)011<3128:MDAERT>2.0.CO;2.

Tanre, D., B. N. Holben, and Y. J. Kaufman (1992), Atmospheric correction algorithms for NOAA-AVHRR products: Theory and application, *IEEE Trans. Geosci. Remote Sens.*, *30*, 231–248, doi:10.1109/36.134074.

Thonicke, K., A. Venevsky, S. Sitch, and W. Cramer (2001), The role of fire disturbance for global vegetation dynamics: Coupling fire into a dynamic global vegetation model, *Global Ecol. Biogeogr.*, *10*, 661–677, doi:10.1046/j.1466-822X.2001.00175.x.

Tweit, S. J. (1995), *Barren, Wild and Worthless: Living in the Chihuahuan Desert*, Univ. of N. M. Press, Albuquerque.

Van Auken, O. W. (2000), Shrub invasions of North American semiarid grasslands, *Annu. Rev. Ecol. Syst.*, *31*, 197–215, doi:10.1146/annurev.ecolsys.31.1.197.

van den Dool, H., J. Huang, and Y. Fan (2003), Performance and analysis of the constructed analogue method applied to U.S. soil moisture over 1981–2001, *J. Geophys. Res.*, *108*(D16), 8617, doi:10.1029/2002JD003114.

Vera, C., et al. (2006), Toward a unified view of the American monsoon systems, *J. Clim.*, *19*, 4977–5000, doi:10.1175/JCLI3896.1.

Vivoni, E. R., H. A. Moreno, G. Mascaro, J. C. Rodriguez, C. J. Watts, J. Garatuza-Payan, and R. L. Scott (2008), Observed relation between evapotranspiration and soil moisture in the North American monsoon region, *Geophys. Res. Lett.*, *35*, L22403, doi:10.1029/2008GL036001.

Vivoni, E. R., C. J. Watts, and D. J. Gochis (2010), Land surface ecohydrology of the North American monsoon system, *J. Arid Environ.*, *74*, 529–530, doi:10.1016/j.jaridenv.2009.11.004.

Wagner, W., K. Scipal, C. Pathe, D. Gerten, W. Lucht, and B. Rudolf (2003), Evaluation of the agreement between the first global remotely sensed soil moisture data with model and precipitation data, *J. Geophys. Res.*, *108*(D19), 4611, doi:10.1029/2003JD003663.

Weiss, J. L., D. S. Gutzler, J. E. Allred Coonrod, and C. N. Dahm (2004a), Long-term vegetation monitoring with NDVI in a diverse semi-arid setting, central New Mexico, USA, *J. Arid Environ.*, *58*, 249–272, doi:10.1016/j.jaridenv.2003.07.001.

Weiss, J. L., D. S. Gutzler, J. E. Allred Coonrod, and C. N. Dahm (2004b), Seasonal and inter-annual relationships between vegetation and climate in central New Mexico, USA, *J. Arid Environ.*, *57*, 507–534, doi:10.1016/S0140-1963(03)00113-7.

Whittaker, R. H., and W. A. Niering (1965), Vegetation of the Santa Catalina Mountains, Arizona: A gradient analysis of the south slope, *Ecology*, *46*, 429–452, doi:10.2307/1934875.

Willmott, C. J., and K. Matsuura (1995), Smart interpolation of annually averaged air temperature in the United States, *J. Appl. Meteorol.*, *34*, 2577–2586, doi:10.1175/1520-0450(1995)034<2577:SIOAAA>2.0.CO;2.

Willmott, C. J., C. M. Rowe, and Y. Mintz (1985), Climatology of the terrestrial seasonal water cycle, *J. Climatol.*, *5*, 589–606, doi:10.1002/joc.3370050602.

Wright, R. G., and G. M. Van Dyne (1976), Environmental factors influencing semidesert grassland perennial grass demography, *Southwest. Nat.*, *21*, 259–273, doi:10.2307/3669712.

Xiao, J., et al. (2008), Estimation of net ecosystem carbon exchange for the conterminous United States by combining MODIS and AmeriFlux data, *Agric. For. Meteorol.*, *148*, 1827–1847, doi:10.1016/j.agrformet.2008.06.015.

Yu, B., and J. M. Wallace (2000), The principal mode of interannual variability of the North American monsoon system, *J. Clim.*, *13*, 2794–2800, doi:10.1175/1520-0442(2000)013<2794:TPMOIV>2.0.CO;2.

S. Collins, Department of Biology, University of New Mexico, Albuquerque, NM 87131, USA.

R. G. Gallimore, Z. Liu, and M. Notaro, Center for Climatic Research, University of Wisconsin-Madison, 1225 W. Dayton St., Madison, WI 53706, USA. (mnotaro@wisc.edu)

D. S. Gutzler, Department of Earth and Planetary Sciences, University of New Mexico, Albuquerque, NM 87131, USA.

J. W. Williams, Department of Geography, University of Wisconsin-Madison, 550 N. Park St., Madison, WI 53706, USA.